Cooling, trap loading, and beam production using a cryogenic helium buffer gas

Wesley C. Campbell John M. Doyle

May 20, 2008

Contents

Trapping and cooling of neutral particles, starting 23 years ago with the first magnetic trapping of an atom [47], has completely transformed the toolbox of atomic, molecular, and optical physics. The breadth of scientific impact is astounding, ranging from creation of new quantum systems, observation of new collisional processes, enhancements in precision measurement techniques, and new approaches to quantum information and simulation. Yet, we feel that the current situation is only a beginning. Compared to the situation with atomic and molecular beams, the number of trapped or cooled species is paltry—no more than 30 different species versus hundreds for beams. With new species come new interactions (and new complications). There is much to look forward to. Examples of "unfinished business" include: creation of polar molecules in optical lattices (predicted to be useful as a tunable Hubbard model system), strongly interacting dipolar gases, dramatic improvements in the search for permanent dipole moments, in-laboratory study of the myriad of astrophysical cold collisional processes, quantum computers based on single atom or molecule qubits, and arbitrary species cooling for precision studies such as variation of fundamental constants (see Chapter by Kozlov and Flambaum). All of these are on the near horizon, thanks to the continued large efforts toward expanding trapping and cooling techniques. The development of these new techniques and their rapid application to new systems has brought a continuing harvest of scientific findings.

This chapter describes the experimental techniques of buffer-gas cooling, loading, and slow beam formation, the latter two building upon the first. Buffer-gas cooling uses a helium refrigerator to cool a gas of helium, which, in turn, cools atoms or molecules. The extraordinary generality and simplicity of buffer-gas cooling results from a combination of 1) helium being chemically inert and effectively structureless, 2) the typical cold elastic cross section of helium with any atom or molecule being around 10^{-14} cm^2 (allowing for centimeter size cooling cells), 3) the appreciable saturated vapor pressure of helium at temperatures down to 200 mK and 4) existing techniques to create gas-phase samples of nearly any species, including radicals.

There are three main sections to this chapter. First, we review buffer-gas cooling, in which hot atoms or molecules are introduced into a cold helium gas, where they thermalize. Second, we discuss buffer-gas loading of traps. Third, we describe production of cold molecular and atomic beams made by adding a hole in the side of the cryogenic buffer-gas cell. These three processes are depicted in Figure 1. Although buffer-gas cooling could be used with other gases to cool to temperatures above 4 K (e.g. H_2 or Ne to temperatures around 15 K), this review covers only buffer-gas cooling to temperatures around and below the boiling point of liquid helium, 4.2 K. Much of the buffer gas physics described in this review would apply to higher temperature systems, especially those using neon.

1 Buffer-gas cooling

The technique of buffer-gas cooling [18] relies on collisions with cold buffer gas atoms to thermalize atoms or molecules to low temperature. The buffer gas serves to dissipate translational energy of the target species and, in the case of molecules, their rotational energy as well. Since this dissipation scheme does not depend on any particular energy level pattern, any target species is amenable to it. As with the case of evaporative cooling of a trapped

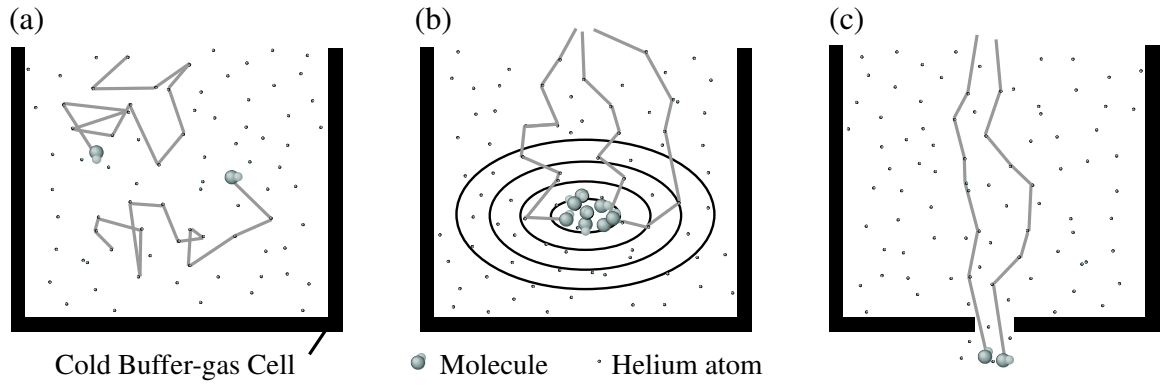

Figure 1: Buffer-gas (a) cooling, (b) loading and (c) beam creation. (a) Buffer-gas cooling occurs when the hot target species **A** (molecules or atoms) enters cold buffer gas inside a cold cell, which are both at a low temperature T. The **A** particles collide with the buffer gas, cooling to a temperature close to T in approximately 100 collisions. The particles of **A** then diffuse to the wall, where they stick and are lost. The sizes of the **A**-He and He-He cross sections determine the efficiency of indirect cooling of **A** by the cell wall after the initial thermalization. (b) In buffer-gas loading, thermalized **A** particles feel a potential due to some type of trapping field (*e.g.* magnetic or electric). The **A** particles in trapping states feel a force pulling them to the center of the trap, whereas those in untrapped (or anti-trapped) states move to the walls where they stick. The time for this "fall in" is about the diffusion time of **A** particles across the cell with the trapping field turned off. (c) Thermalized **A** particles can exit a hole in the side of a cryogenic cell and form a cold beam of **A**. The extraction efficiency and velocities of **A** in the beam depend on the density of helium, size of the cell and size of the exit hole.

ensemble, buffer-gas loading relies on elastic collisions.

At temperatures of ~ 1 K, all substances except for He (and certain spin-polarized species, such as atomic hydrogen) have negligible vapor pressure, so the question arises as to how to bring the species-to-be-cooled into the gas phase and then into the buffer gas. Five methods have been used to accomplish this: laser ablation, beam injection, capillary filling, discharge etching and laser-induced atom desorption (LIAD).

The translational thermalization process of the target species with cold helium can be modeled by assuming elastic collisions between two mass points, m (buffer gas atom) and M (target species). From energy and momentum conservation in a hard-sphere model, we find, after thermal averaging, that the difference, ΔT, in temperature of the atom or molecule before and after a collision with the buffer gas atom is given by $\Delta T = (T' - T)/\kappa$, with T denoting the temperature of the buffer gas, T' the initial temperature of the atom or molecule, and $\kappa \equiv (M + m)^2/(2Mm)$. The equation for the temperature change can be generalized and recast in differential form:

$$\frac{\mathrm{d}T_\ell}{\mathrm{d}\ell} = -(T_\ell - T)/\kappa \tag{1}$$

where T_ℓ is the temperature of the atom or molecule after ℓ collisions with the buffer gas atom. Eq. 1 has a solution

$$T_\ell/T = (T'/T - 1)e^{-\ell/\kappa} + 1. \tag{2}$$

Under the conditions of $T' \approx 1000$ K and $M/m \approx 50$, of order one hundred collisions are required for the atoms or molecules to fall to within 30% of the He buffer-gas temperature $T = 0.25$ K. 100 collisions typically corresponds to a time of order 0.1–10 ms, depending on the buffer-gas density; this is consistent with our observations of buffer-gas cooling. Fig. 3 shows the thermalization of laser-ablated VO in cold helium buffer gas for different delays after the ablation pulse. The spectra show complete translational thermalization in less than 10 ms, in accordance with the above simple model.

In order to ensure that the target species thermalizes before impinging on the wall of the cell, it is necessary that the density of the buffer gas be large enough to allow for thermalization on a path smaller than the size of the cell. Cells are typically of order 1 cm in diameter. Assuming an elastic collision cross section of about 10^{-14} cm^2 between the target species and helium (an assumption accurately borne out by numerous experiments [36, 68, 69, 12]), the minimum density required is typically 3×10^{14} cm^{-3}. This requirement puts a lower limit on the temperature of the buffer gas. Figure 2 shows the dependence of number density on temperature for ^{3}He [33] and ^{4}He [59] at about 1 K. One can see that ^{3}He can be used at temperatures as low as 180 mK and ^{4}He as low as 500 mK.

In the above discussion of thermalization, it was assumed that the temperature of the buffer gas was fixed to its final temperature (typically around 1 K). For short times (less than the diffusion time of helium to the cell walls) one must consider the heat capacity of the buffer gas, *i.e.* when there is no other mechanism present to take energy away from the hot molecules. To cool to a temperature within 30% of T, the ratio Υ of the minimum number of (pre-cooled) helium atoms to the number of initially hot (T') target species is given by $\Upsilon = (T'/T - 1)/0.3$. For $T \approx 4$ K and $T' \approx 1000$ K this amounts to $\Upsilon \approx 1000$. This is a kind of "worst case". Depending on the experimental set-up, goals, and elastic cross sections, it

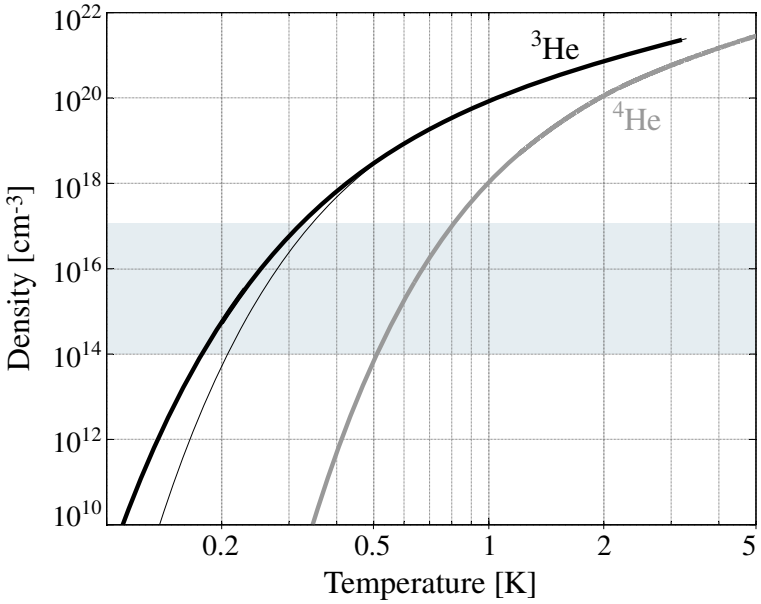

Figure 2: The saturated vapor density of helium at buffer-gas cooling temperatures. The ^{4}He curve is extrapolated from ITS-90 [59] and the ^{3}He curve is from [33] with the old ITS-90 curve (thin line) shown for reference. The shaded region represents the range of saturated vapor densities used for buffer-gas loading, which sets a minimum temperature of 180 and 500 mK for ^{3}He and ^{4}He buffer gas, respectively.

may be possible to use the cold walls of the chamber to cool the buffer gas with little loss in the number of molecules. This is especially true while, for example, molecules are being drawn through the buffer gas into the center of a magnetic trap.

1.1 Loading of species into the buffer gas

We know of five demonstrated species introduction methods (the first four of which have been used in our laboratory): laser ablation, beam injection, capillary filling, discharge etching and LIAD. A schematic of the first four methods is depicted in Fig. 4.

1.1.1 Laser ablation and LIAD

Numerous species have been laser-ablated and buffer-gas cooled. Laser ablation of solid materials is well established as an important tool in many scientific and technological endeavors, including surface processing, surgery, mass spectrometry and growth of materials. Despite prolific applications, sorting out the fundamental mechanisms for laser ablation and identifying all the physical processes involved in laser ablation has proven quite difficult. For example, the coupling mechanism between the laser light and the sample can be very complex since the optical and thermal properties may change upon laser exposure due to formation of excited states and plasma. These processes become even more complicated and essentially intractable when chemical reactions are required to produce the species of

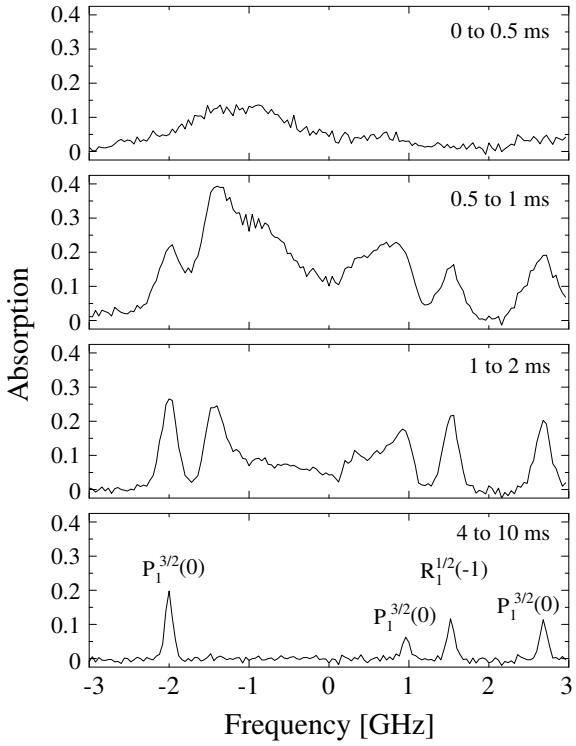

Figure 3: Laser absorption spectra showing the thermalization of laser-ablated VO in helium buffer gas. The molecules thermalize to the temperature of the cell walls in less than 4 ms. Reprinted with permission from [67].

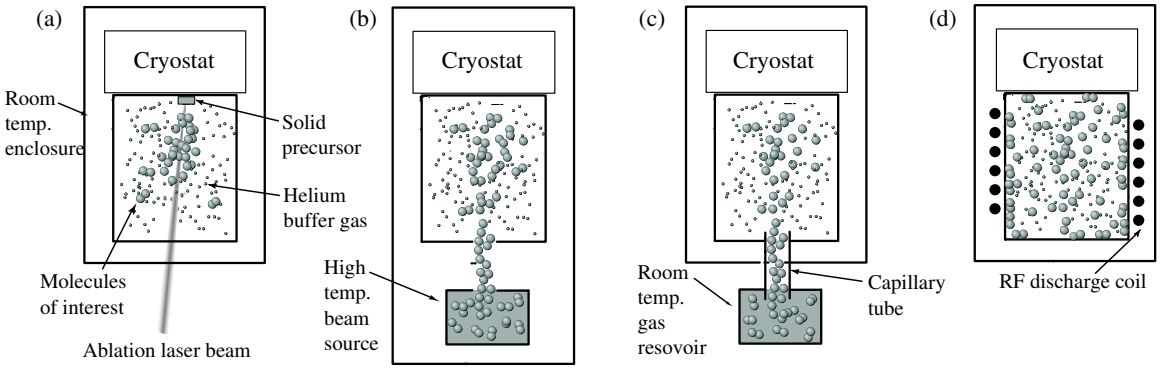

Figure 4: Introduction of molecules into the buffer gas through (a) laser ablation of a solid precursor, (b) molecular beam injection, (c) capillary injection and (d) discharge etching.

interest. For example, CaF, CaH and VO radicals were produced by the same 532 nm (4 ns pulse length, approximately 10 mJ energy) laser ablation of stable solids, CaF_2, CaH_2 and V_2O_5, respectively. The yields, however, varied by 5 orders of magnitude. In the case of CaH, only 10^{-8} of the pulse energy went into breaking the single chemical bond to produce CaH from CaH_2. Because of the heating limitations of buffer-gas cooling, the pulse energies used are typically below 20 mJ.

LIAD is a laser-induced desorption process that has been demonstrated exclusively with atomic Rb and K. We refer the reader to reference [31] for more details. In short, laser light excites a plasmon resonance in the solid metal, driving atoms off the surface and into the buffer gas.

1.1.2 Beam injection

Beam injection is perhaps the most general way of introducing target species into a cold buffer gas. However, it is also the most difficult. The idea is to have an orifice in the side of the buffer-gas cell, typically millimeter to centimeter size, to allow a beam of molecules or atoms to pass into the cell. Making beams of essentially any atom or molecule is possible. The density of helium in the cell is not high enough to form clusters (at least for atoms and simple molecules). However, with the addition of the molecular beam input orifice, a new host of problems arises. First, the escaping helium can build up density just outside the cell, knocking incoming molecules out of the molecular beam, preventing them from entering the cell. Second, even if the molecules enter the cell, they may be hydrodynamically pulled back out of the cell as helium is continually moving through the orifice into the vacuum region. Third, helium must continually be replenished, adding a potential heat load to the cryogenic system. Despite these difficulties, we have been able to show efficient beam injection loading and buffer-gas cooling of Rb, N, NH, and ND_3, including trapping of N and NH and electric guiding of ND_3 (see Appendix). The key to success was rapid pumping of the buffer gas in the beam region (outside the orifice) via a cryogenic sorption pump for helium made of charcoal.

1.1.3 Capillary filling

Capillary filling is, perhaps, the first idea that comes to mind when thinking about how to introduce atoms or molecules into a buffer gas. Indeed, it was the first method used to buffer-gas cool a molecule [45]. In essence, it is guiding using solid walls. Gas phase species are transported from high temperature (typically at or above 300 K) to 4 K via a fill capillary. This arrangement has its own peculiar technical problems. First, because one end of the fill capillary is exposed to 4 K buffer gas, not only is there a heat load from the tube into the buffer gas, but the tube near the buffer-gas cell could become cold enough to freeze the incoming species. Second, since species require the fill tube to be maintained above their freezing point, most species require temperatures at or above room temperature, which can become a problem due to the cell capillary depositing heat into the cold buffer-gas cell. Third, depending on the flow conditions the species coming down the tube can suffer intra-species collisions and collisions with the walls of the tube. As such, this method may be of limited utility for chemically reactive species. However, it is possible to partially

overcome the wall issues by using high enough flow of gas through the capillary so that the target species does not hit the tube wall before entering the cold cell. One variation on this approach is co-flow of an inert gas in the capillary. If the flow is rapid enough, the diffusion time of a molecule through the inert gas to the wall of the capillary can be less than the time the molecule spends in the capillary (the "residence time"). One can show that the condition for the diffusion time to be equal to the residence time in a capillary of length $\mathcal{L}$[cm] and with a flow rate $\dot{N}$[sccm] is approximately given by $\mathcal{L} \approx 0.1\dot{N}$ at $T \approx 4K$.

Without resorting to co-flow the capillary method is generally limited to a small subset of atomic and molecular species. However, that small subset contains some very important molecules, including O_2, NH_3, HCN, and N_2. Although in principle atomic samples could be introduced into a buffer-gas cell through a heated capillary (particularly for low boiling point metals like Hg and Cs), to our knowledge no atom has ever been buffer-gas cooled using capillary filling.

1.1.4 Discharge etching

A final method for introducing species into the cold buffer gas is discharge etching, in which an electrical discharge plasma in the buffer gas "etches" off species that are frozen to the cell wall, bringing them into the gas phase. Once liberated, the discharge plasma can even excite/dissociate a fraction of them (*e.g.* into a metastable state). To date we have only used this for one species, He*, but based on the success with He* and previous work with low-temperature production of atomic hydrogen, it is likely that this method will find further application. The type of discharge used for this purpose in our lab is a $\lambda/4$ RF helical resonator coil discharge. The coil is wound around or inside the buffer-gas cell [16].

Our He^* experiments begin with an entirely empty cell whose inner surface has been precoated with a few monolayers of atomic helium with one end open to high vacuum. The helium on the walls of the cell is naturally tightly bound to the surface as all the weakly bound helium has already been pumped away. A short RF pulse (typically 300 μs) is sent to the discharge coil. The discharge ignited, pulling enough helium atoms off the surface to act as a buffer gas. A small fraction of the helium (about 10^{-5}) is turned into metastable (magnetic ^3S-state) helium and is buffer-gas cooled. About 5×10^{11} metastable helium atoms are created, buffer-gas cooled, and magnetically trapped in this way [16].

1.2 Rotational and vibrational relaxation

A central issue with the technique of buffer-gas cooling of molecules is the efficiency of cooling rotational, vibrational, spin or other internal degrees of freedom. For experiments limited by counting statistics, cooling of these degrees of freedom may be critical due to the drastic effect such cooling can have on the population of molecules in the desired state. It may also be desirable to use the buffer gas to cool only specific degrees of freedom while leaving others out of thermal equilibrium. Applications of this kind of selective thermalization include buffer-gas loading of magnetic traps (described in section 2) where the electron spin temperature must remain thermally disconnected from the buffer-gas temperature. In order to assess the feasibility of such experiments, the timescales for relaxation must be understood.

Generally, collision-induced quenching is far more efficient for rotation than vibration. Rotational quenching is driven by the angular anisotropy of the helium interaction with the molecule, and the timescale for a small impact parameter cold collision is similar to a rotational period. Vibrational relaxation, on the other hand, is driven by the dependence of the interaction potential on the internuclear separation in the molecule. The vibrational motion of the nuclei, being characterized by typical energy separations of 1000 K, is much faster than a cold helium atom collision.

Typical quenching cross sections by cold (~ 1 K) helium yield a rotational quench on the order of every 10-100 elastic collisions whereas it can take more than 10^8 elastic collisions before a vibrational quench [22]. DeLucia and co-workers measured rotationally inelastic cross sections with He of H_2S, NO, and H_2CO. Typical values were on the order of 1-10×10^{-16} cm^2 at 1 K [4, 5, 44], which is about 10-100 times smaller than a typical diffusive cross section at 1 K. We therefore expect buffer-gas cooling to effectively thermalize the rotational temperature of the target molecules while leaving the vibrational temperature out of thermal equilibrium. Since the rotational and translational energy transfer cross sections are similar, thermalization of both happens rapidly and in tandem in buffer-gas cooling. We do not detect non-equilibrium rotational populations.

Vibrationally hot molecules, on the other hand, have been created using laser ablation and molecular beam loading and have been observed in our group. We were able to translationally cool CaH($v = 1$) to < 500 mK and saw no evidence of vibrational quenching, giving a limit of $\sigma_{\mathrm{CaH},v=1} < 10^{-18}$ cm^2 on the helium induced vibrational quenching cross section [68]. We also magnetically trapped NH($v = 1$) and found that the lifetime of the trapped vibrationally excited molecules was limited by spontaneous emission, not collisional thermalization. The fact that the vibrational temperature remained extremely hot allowed us to perform a precise measurement of the NH($X^3\Sigma^-, v = 1 \rightarrow 0$) spontaneous emission lifetime. We measured a limit of $k_{\mathrm{NH},v=1} < 3.9 \times 10^{-15}$ cm^{3}s^{-1} for the helium induced vibrational quenching coefficient [10].

2 Buffer-gas loading of magnetic traps

Buffer-gas loading can take place when buffer-gas cooling occurs within a trapping potential. Using the language of magnetic traps, the low-field seekers (LFS, meaning those states whose Zeeman energy increases with increasing magnetic field) cool to the temperature of the buffer gas and feel a force drawing them to the center of the trap (where the field magnitude is a minimum). This "fall-in" process takes place on a time scale comparable to the field-free diffusion time of molecules in the buffer gas. Depending on the helium density and initial conditions, this can take place over $N_{fall-in} = 10$-10^4 collisions. The high-field seekers (HFS) are, in contrast, pushed out to the edge of the trap on about the same timescale, where they stick to the cold walls and are lost from the trapping region.

In order for trapping to work, the temperature of the buffer gas must be lower than the trap depth and the low-field seekers must not change to other (energetically favorable) states as they diffuse to the center of the trap and form a trapped distribution. As such, if there is an inelastic process such as reorientation of the magnetic moment of the molecule due to a collision with helium, the molecule may be lost before trapping occurs. The ratio of diffusion

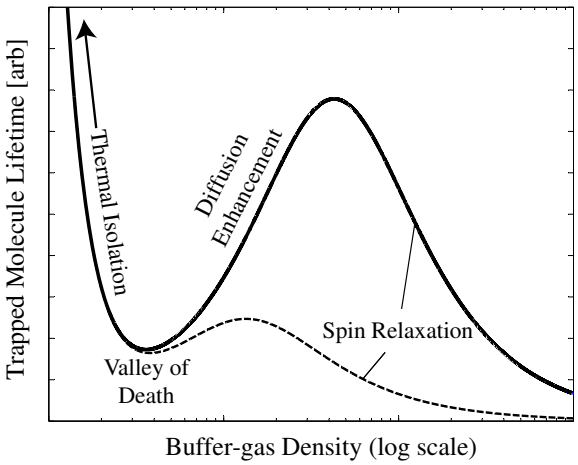

Figure 5: Trapped molecule lifetime vs. buffer-gas density (note semilog scale) for two hypothetical molecular species. For the dashed curve, the helium-induced Zeeman relaxation cross section has been increased by a factor of 10.

(elastic) to inelastic cross sections, γ, for helium colliding with the target species must be above a certain value for trapping to take place, $\gamma > N_{fall-in}$.

2.1 Lifetime of trapped molecules

The lifetime of a trapped sample may be limited by collisions with the helium buffer gas. Fig. 5 schematically shows the lifetime of two hypothetical trapped molecular species. Four distinct regimes are represented, each with a different physical mechanism that limits the trap lifetime. Elastic collisions with helium can promote molecules to energies above the depth of the trap (evaporative loss, occurring near the "Valley of Death" and in the "Diffusion Enhancement" regions indicated in Fig. 5). Helium collisions can also inelastically change the internal state of the molecule to an untrapped state, which limits the trap lifetime in the section of Fig. 5 marked "Spin relaxation." The removal of the buffer gas is necessary in order to shut these processes down to obtain a thermally isolated sample that could be cooled to a temperature below that of the cell walls. This is shown in the area labeled "Thermal Isolation," where the rate of He collisions is low, leading to long trap lifetimes and low heating rates for the trapped sample. A comparison of the lifetime of the trapped molecules to the pump-out time of the buffer gas out of the cell serves as a guide for the feasibility of achieving thermal isolation.

2.1.1 Evaporative loss

A thermal Boltzmann trap distribution of molecules always contains molecules whose energies allow them to access the spatial edge of the trap. As molecules reach this edge and stick to the cold walls of the buffer-gas cell, a truncation of the distribution takes place. Molecules that pass the edge of the trap are lost from the distribution and this evaporative loss can be the limiting factor in determining the lifetime of trapped molecules.

The evaporation-limited lifetime of trapped molecules depends sensitively on η, the trap depth measured in terms of the molecules' translational energy

$$\eta \equiv \frac{\mu B_{\max}}{k_{\mathrm{B}} T}. \tag{3}$$

In the long mean free path regime, the average total distance λ traveled before the molecule's trajectory is randomized by a collision (the diffusion mean free path) is large compared to the size of the trap. A lower limit for the evaporation-limited long mean free path trap lifetime can be estimated by assuming ballistic travel through the trap and a distribution of molecules that is continuously thermalized to the temperature of the cell walls. (This situation occurs in the "Valley of Death" region of Fig. 5.) The evaporation rate is then given by flux of molecules to the trap edge, $\phi = (1/4) n \bar{v}$. This yields the expression

$$\tau \geq \frac{4 V_{\mathrm{eff}}}{\bar{v}_{\mathrm{molec}} A} e^{\eta} \tag{4}$$

where V_{eff} is the "effective volume" of the trap (the ratio of the total molecule number to peak molecule density), $\bar{v}_{\mathrm{molec}}$ is the average velocity of the molecules and A is the surface area of the trap edge [18]. For a spherical quadrupole trap (such as the anti-Helmholtz traps used in our group) whose depth is set by the radius of the cell, r_0, we have $V_{\mathrm{eff}} \approx 2.7 \times V_0/\eta^3$ (where $V_0 = 4/3\pi r_0^3$).

The long mean free path evaporation described by Eq. 4 is the limiting loss mechanism at low helium density, where the assumption of ballistic travel through the trap is valid. At higher buffer-gas densities, where $\lambda < r_0$, the helium enforces diffusive motion of the molecules in the trap, which slows the evaporation rate and therefore increases the trap lifetime, as shown in the "Diffusion Enhancement" section of Fig. 5. It is in this short mean free path regime that buffer-gas loading typically begins, and the modeling of the lifetime is somewhat more complicated than in the long mean free path regime.

Starting with the field-free diffusion lifetime, the trap lifetime can be obtained by solving the diffusion equation with the boundary condition that the molecule density be zero at the walls of the cylindrical cell. The lifetime of the lowest-order field-free diffusion mode is given by

$$\tau_0 = \frac{16 n_{\mathrm{He}} \sigma_{\mathrm{d}}}{3\sqrt{2\pi}} \sqrt{\frac{m_{\mathrm{red}}}{k_{\mathrm{B}} T}} \left[\left(\frac{\alpha_1}{r_0} \right)^2 + \left(\frac{\pi}{h_0} \right)^2 \right]^{-1} \tag{5}$$

where σ_{d} is the thermal average of the diffusion cross section, r_0 and h_0 are the internal radius and length of the buffer-gas cell, m_{red} is the reduced mass of the collision complex and $\alpha_1 \approx 2.40$ is a numerical factor [30].

The effect of the trapping field can be accounted for by numerically solving the diffusion equation with a drift term from the trap [70]. Fig. 6 shows the calculated lifetime using this approach (in units of the field-free diffusion lifetime, τ_0) as a function of η. As can be seen from Fig. 6, for $\eta > 6$, the trapping lifetime is 10 times greater than the field-free diffusion time.

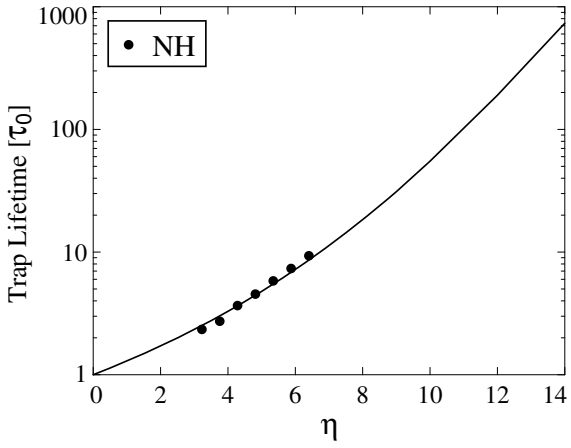

Figure 6: Trapped molecule lifetime vs. trap depth in units of the field-free diffusion lifetime, τ_0 (Eq. 5). The points are data taken for NH [12].

2.1.2 Buffer gas removal

In the regime where the trap lifetime is limited by evaporation (the long mean free path regime, section 2.1.1), the presence of the buffer gas *shortens* the trapped molecule lifetime. This is because the constant rethermalization of the trapped sample to the buffer-gas temperature continuously promotes molecules to energies above the trap edge. If all collisions could be turned off, the trapped molecules with total energy lower than the trap depth would stay in the trap for an extended period of time, indicated as "Thermal Isolation" in Fig. 5. In this regime, the trapped molecule lifetime would likely become limited by longer timescale effects, such as Majorana transitions or molecule-molecule collisions.

One way to achieve this thermal disconnect is to remove the buffer gas. This can be done either by cooling the cell walls [69] to lower the saturated vapor density of helium (see Fig. 2) or by pumping the gas out through an orifice in the side of the cell [29]. In order for the molecule number after buffer gas removal to be large, the timescale for pump-out must be small compared to the "Valley of Death" lifetime in Fig. 5.

Such a pump-out can introduce two new complications. First, a helium film on the walls of the cell can desorb slowly, leading to longer times spent in the "Valley of Death". The binding energy of the first (bottom) monolayer is typically of order 100 K and the timescale for desorption at 500 mK is extremely long. The binding energy of the least bound (top) monolayer is on the order of the cell temperature and therefore rapidly desorbs during the cell pump-out. The difficulty occurs with the layers in between, which desorb on the timescales of experiments, effectively softening the vacuum and maintaining the buffer-gas density near the valley of death, as shown in Fig. 7. To combat this problem, the temperature of the cell can be lowered after some desorption, meaning that buffer-gas loading should occur above the base temperature of the refrigerator. This sort of heating while pumping is well known to the room-temperature UHV atom trapping community as a *bakeout*. A typical *cryo-bakeout* involves a temperature rise of less than 1 K above base temperature.

The second possible complication is the helium wind pulling the trapped molecules out of the trapping region. We have studied this effect as well and found that fortunately, it is

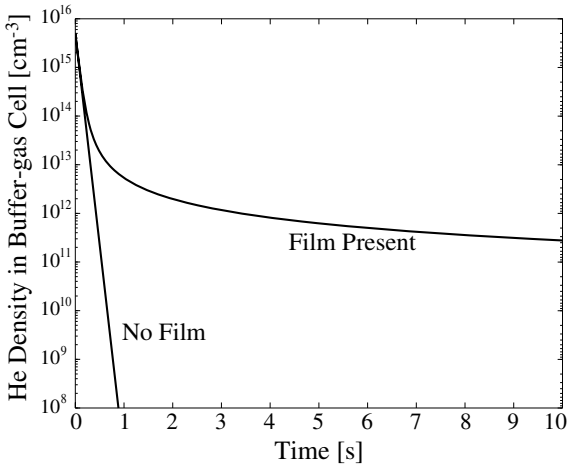

Figure 7: Calculated helium buffer-gas density vs. time after opening a high-conductance valve to pump out the cell [46]. The rapid pump-out in the absence of a film is compromised by the slow helium film desorption.

possible to avoid it in most circumstances [46].

2.1.3 Spin relaxation loss (atoms)

A significant drawback of trapping via a low-field seeking (LFS) Zeeman sublevel is that this opens an exothermic inelastic collision channel. During a collision, a stretched-state[1] LFS molecule can undergo a Zeeman transition to a less-trapped or even high-field seeking (HFS) state. This process is referred to as either "Spin Relaxation[2]" (as in Fig. 5) or collision-induced Zeeman relaxation. To utilize buffer-gas loading to trap a species, this process must be sufficiently unlikely that the external motion of the molecule can be thermalized and the experiment carried out before the Zeeman state changes.

All of the inelastic collision processes seen in atoms are also possible with molecules, and they are categorized here to distinguish them from processes unique to molecules. Collision-induced Zeeman transitions in atoms can be induced by spin-exchange, dipolar relaxation, interaction anisotropy, Feshbach resonances, metastable decay, shape resonances, and three-body recombination. The last of those will not be treated here since achievable cold polar molecule densities are currently far too low for three-body collisions.

In spin-exchange, an atom with a net spin can trade angular momentum with the spin of its collision partner. This is not a factor for collisions with ground-state ^{4}He since it has zero spin, but the ^{3}He nuclear spin and any other atom with net angular momentum can potentially participate in spin-exchange collisions. The dominant mechanism for alkali atom spin-exchange with ^{3}He is the overlap of the alkali valence electron with the ^{3}He nucleus, which results in a (molecular-type) hyperfine interaction. Spin-exchange cross sections for alkali atoms colliding with ^{3}He at room temperature are typically 10^9 times smaller than the

[1] $m_J = \pm J$

[2] We will focus here on the case where the magnetic moment comes entirely from electron spin, although it is possible for the magnetic moment to have contributions from electron orbital angular momentum.

elastic cross section [64], and should be no larger for molecule-^{3}He collisions.

Dipolar relaxation also requires both collision partners to have magnetic moments. Although it is not a major concern for collisions with helium, it is ubiquitous in magnetically trapped samples. Briefly, the spin-spin interaction (which will be described in detail in the treatment of $^3\Sigma$ molecules) between magnetic moments of two colliding particles can exchange angular momentum between the electrons and the relative motion of the particles. This can arise as a result of the magnetic dipole-magnetic dipole interaction (which dominates for light particles) or as a result of a second-order interaction with a nonzero electron orbital angular momentum state (which tends to dominate for heavy particles). Dipolar relaxation rate coefficients are typically smaller than 10^{-13} cm^{3}s^{-1}.

The interaction between the atom of interest and a helium atom (V_{He}) does not couple directly to the electron spin projection. This is in contrast to magnetic particles, which can cause Zeeman transitions through the spin-spin interaction. The long-range part of the helium interaction is typically dominated by the van der Waals potential and can be thought of as being an electrostatic interaction (though the short range portion involves exchange-type interactions). There is essentially no first-order probability for this to cause a spin reprojection:

$$\langle S, M_S \left| V_{\mathrm{He}} \right| S, M_S' \rangle \propto \delta_{M_S M_S'}. \tag{6}$$

The helium atom can, however, distort the *spatial* charge cloud. In this respect, both the radial and angular wavefunctions of the electrons must be considered. We will concentrate first on the angular charge distribution, some examples of which are depicted in Fig. 9. For atoms, the angular distribution of electron charge is governed by the electron orbital angular momentum state $|L, M_L\rangle$. For atoms with nonzero electron orbital angular momentum, the helium interaction can introduce an admixture of different M_L states, which can be thought of as the exertion of a torque on the electron cloud. The spin-orbit interaction in the atom ensures that this admixing of M_L states is accompanied by an admixing of M_S states, potentially driving a Zeeman transition.

S-state atoms, on the other hand, have only $M_L = 0$ and are spherically symmetric. In order to drive Zeeman transitions, the helium atom must first mix in a state with nonzero electron orbital angular momentum, such as a p orbital. The energy splitting between these states tends to be much larger than the helium interaction energy. Numerous S-state atoms have been buffer-gas cooled and loaded into magnetic traps: He*, Cr, Mo, Mn, Na, Li, Cu, N, Ag, Eu. Only with Ag and Cu was γ small enough to be measurable in the experiments [35].

It is expected that atoms in non-S-states suffer inelastic collision loss rates much higher than S-state atoms. Indeed, calculations indicate that the main-group non-S-state atoms Sr(P), Ca(P), and O(P) have $\gamma \approx 1$ [38, 37, 61]. Furthermore, it has been observed that nominal S-state atoms that mix in large amounts of non-S shells have relatively low values of γ. Bi is the most prominent of these, with a measured $\gamma < 5 \times 10^4$ [43]. The overall picture of non-S-state atoms having low γ therefore rests on strong experimental and theoretical footing.

There are important exceptions to this well-founded characterization of non-S-state spin relaxation. Due to the non-trivial behavior of the radial part of the electron wavefunction in many atoms, there is a collisional shielding that occurs. Specifically, if the partially-filled

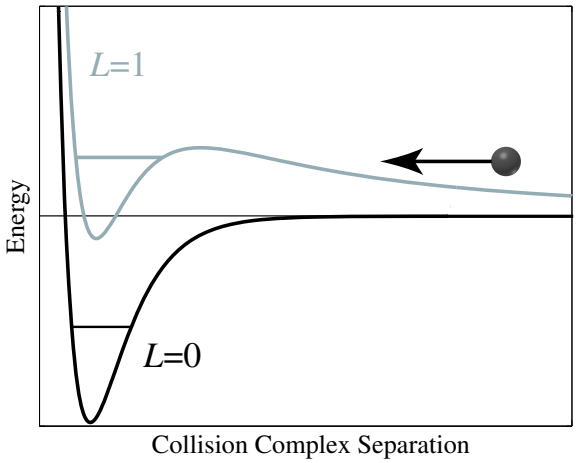

Figure 8: An $L = 1$ shape resonance can occur if the energy of the incoming particle matches the quasi-bound state of the $L = 1$ potential.

orbitals of a non-S-state atom lie closer to the nucleus than an outer filled s-orbital, there is an effective shielding of the anisotropy. Many rare earth (and some transition-metal) atoms exhibit such *submerged shell* structure [23]. The recognition of such structure as a possible suppression agent for spin relaxation in cold collisions led our group to pursue and demonstrate trapping of non-S-state atoms [27, 26]. We found that in the case of the rare earth atoms, in which unpaired electrons are shielded by 2 filled outer s-shells, the shielding was dramatic. This resulted in $\gamma > 10^4$ (and as high as $\approx 10^6$) for Tm, Er, Nd, Tb, Pr, Ho, and Dy, all in states with nonzero electron orbital angular momentum [27]. For the transition metal atom Ti, we found that even a single filled s-orbital effectively shields the unfilled d-orbital, resulting in $\gamma = (4.0 \pm 1.8) \times 10^4$ [26].

There can be an enhancement of the Zeeman transition probability if the interaction time between the trapped species and helium is extended by the formation of a quasi-bound complex, as is the case for a shape resonance (see Fig. 8). If the temperature of the colliding particles is high enough to permit non-s-wave collisions between particles, there may be quasi-bound states with nonzero angular momentum with lifetimes longer than a typical collision duration. The two particles stuck in such a quasi bound state can orbit each other, forming a long-lived complex that increases the likelihood of Zeeman transitions in the species of interest due to the perturbations induced by the other particle. The probability of this occurring is maximized when the kinetic energy of the particles is equal to the energy of the quasi bound state above the dissociation threshold. Shape resonances are very common in the few-partial-wave regime typical of buffer-gas cooling, and their effect on Zeeman relaxation is an active field of study [12, 11].

Another type of resonant interaction that can lead to trap loss is a Feshbach resonance, which can occur through coupling to a true bound level of a higher-energy state of the collision complex. If the total energy of this bound state matches the energy of the colliding atoms, an enhancement of the inelastic rate can occur. Feshbach resonances have come into prominence in the field of cold molecules due to their usefulness for making ultracold molecules from laser-cooled atoms.

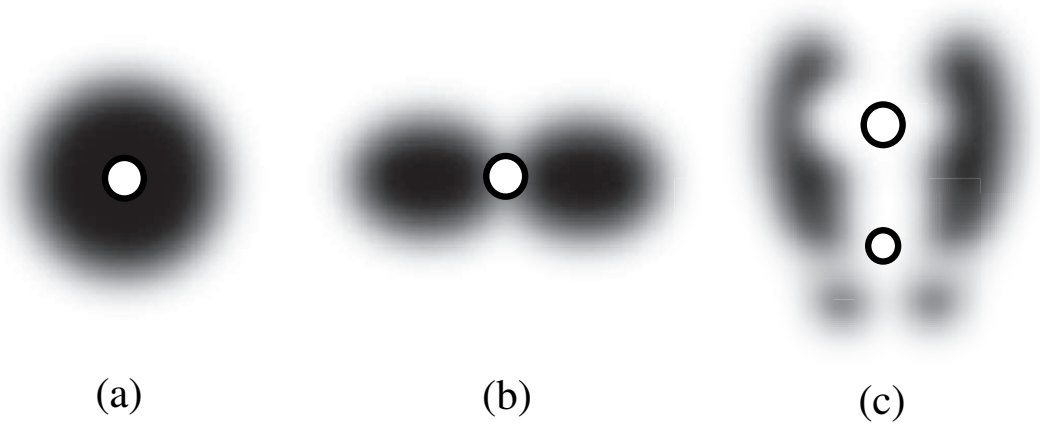

Figure 9: Cartoon depiction of the angular charge distribution in (a) an S-state atom, (b) a P-state atom, and (c) the rest frame of a diatomic molecule.

2.2 Zeeman relaxation collisions between molecules and helium

All of the mechanisms described above for atoms can and do lead to helium induced Zeeman relaxation of diatomic molecules. There are, however, additional pathways leading to trap loss that are unique to molecules. Figure 9(c) shows a hypothetical electron charge density for a diatomic molecule in the rest frame of the molecule. Comparison to Fig. 9(a) and (b) suggests that a similar argument of helium induced Zeeman relaxation would be catastrophic to the potential of buffer-gas loading molecules. The tremendous anisotropy between the molecule and the helium atom leads to a potential minimum at some angle with respect to the internuclear axis, which would allow an incoming helium atom to exert a torque on the molecule.

There is, however, an important difference between Fig. 9(c) and Fig. 9(a) and (b). (a) and (b) are eigenstates of J_Z, the lab-frame projection of the total angular momentum. The molecule-fixed frame electron charge distribution, however, is not and the rotational motion of the nuclei in the lab frame must be taken into account. This degree of freedom is described by the rotational wavefunction, which gives the probability amplitude for finding the internuclear axis pointing in a particular direction (θ, ϕ) on the lab-frame. We can write the rotational wavefunction in terms of R, the rotational quantum number of the nuclei:

$$|R, M_R\rangle = f_{R,M_R}(\theta, \phi) \tag{7}$$

where f is a function of the angles between the internuclear axis and the lab-fixed coordinate system (a rigid rotor wavefunction). Thus we find that even though there is a strongly anisotropic potential between the helium atom and the molecule in the molecule-fixed frame, this potential is averaged over the rotational wavefunction in the lab frame, where the interaction with the helium atom takes place. The strong molecule-fixed frame anisotropy depicted in Fig. 9(c) is therefore effectively shielded from the helium atom by the rotation of the molecule in the lab frame.

A sampling of rotational probability distributions are shown in Fig. 10. The distance

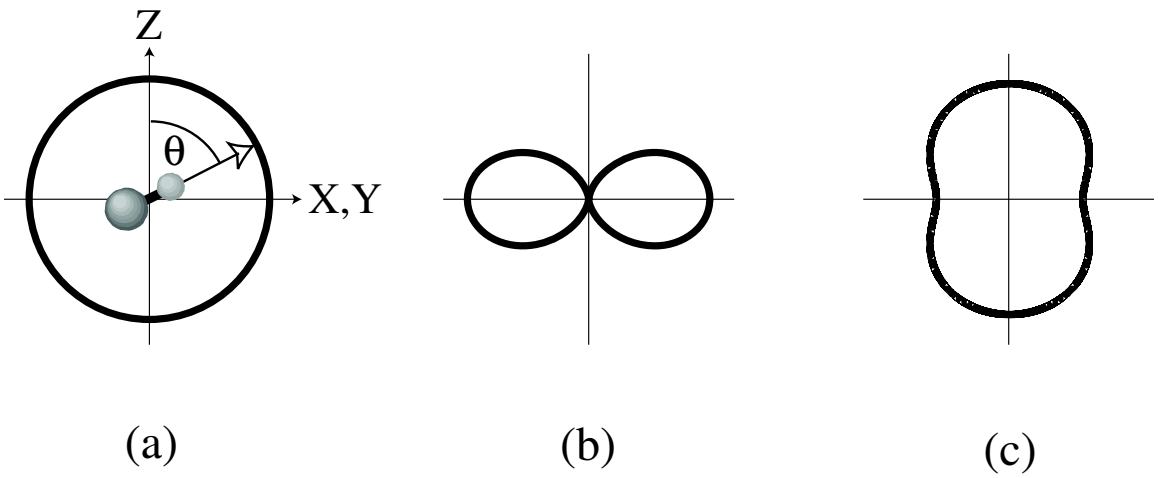

Figure 10: Cartoon depiction of the probability distribution that the internuclear axis makes an angle θ with the lab-frame Z-axis. Distance from the origin (times $\sin\theta \mathrm{d}\theta$ if we wish to average over the polar angle ϕ) is the probability for the rotor to be pointing in the range $\theta, \theta + \mathrm{d}\theta$ for (a) an $|R = 0, M_R = 0\rangle$ state molecule, (b) an $|R = 1, M_R = 1\rangle$ state, and (c) a rotational ground state $^1\Pi$ molecule.

from the origin is the relative probability for the internuclear axis to be oriented at an angle θ with respect to the lab-frame Z-axis. It can immediately be seen that the pure $|R = 0, M_R = 0\rangle$ ground state shown in Fig. 10(a) is spherically symmetric, much like the S-state atom depicted in Fig. 9(a). Likewise, the first excited rotational state $|R = 1, M_R = 1\rangle$ is highly non-spherical, similar to the P-state atom shown in Fig. 9(b). It is therefore reasonable to expect a pure $R = 0$ state to be less likely to undergo helium-induced Zeeman relaxation than an $R = 1$ state, which exhibits significant anisotropy in the lab frame. It is the manipulation of the *rotational* wavefunction by the helium interaction that governs collision-induced Zeeman relaxation of molecules.

The analogy between L in atoms and R in molecules can be understood by thinking of an atom as an ionically bonded molecule where the valence electron is one "ion" and the rest of the atom is the other. The angular wavefunction of the electron $|L, M_L\rangle$, then, is nothing more than the rotational wavefunction $|R, M_R\rangle$ of this pseudo-molecule, and indeed they are described by the same spherical harmonics.

The conclusions that can be drawn from this analysis are very similar to those that were drawn for atoms. For buffer-gas loading, it is desirable to reduce the anisotropy between the molecule and the helium atom. The most "spherical" molecules are those with pure $|R = 0\rangle$ rotational ground states. Rotationally excited states and molecules with significant admixtures of $R \neq 0$ should be more likely to spin-relax. This immediately eliminates molecules with $\Lambda \neq 0$, since the rotational ground states for such molecules contain significant $R \neq 0$ contributions, as shown in Fig. 10(c). Furthermore, the presence of the nearby Λ- or Ω-doublet state of opposite parity is likely to be close enough in energy to be easily mixed in by the Stark effect caused by the helium atom, further increasing the anisotropy. For these reasons it is expected that Σ states will be far more robust against helium-induced Zeeman

relaxation than molecules in states with $\Lambda \neq 0$.

It is still true that choosing molecules with reduced anisotropy in the molecule-fixed frame is beneficial. After all, if there is no anisotropy in the molecule-fixed frame, the helium interaction in the lab frame is spherical for all rotational states. It is therefore desirable to seek molecules with short bond lengths, which should reduce the anisotropy of the electron charge cloud in the molecule frame for a fixed helium approach distance. There is potential for the Zeeman relaxation of superficially anisotropic molecules to be suppressed by spatially large, roughly spherical electron wavefunctions, much like was found with the submerged-shell rare earth elements.

With this understanding in place, is is necessary to examine the properties of magnetic Σ state molecules that lead to Zeeman relaxation in order to assess the feasibility of buffer-gas loading of molecules.

2.2.1 Inelastic collisions of $^2\Sigma$ molecules with He

The simplest paramagnetic molecular state with $\Lambda = 0$ is $^2\Sigma$. The rotational quantum number N is equal to R from the above discussion and we will from here forward use N for the discussion of nuclear rotation, in accordance with standard notation for Σ states. The lone valence electron contributes 1 μ_B of magnetic moment, making $^2\Sigma$ molecules suitable for trapping. The rotational ground state of $^2\Sigma$ is a pure $|N = 0\rangle$ state, which eliminates helium-induced Zeeman relaxation from first-order effects, in accordance with Eq. 6. In order to change the spin projection M_S, there must be a mechanism by which the spin can be coupled to the rotational wavefunction, which can be altered by the electrostatic interaction.

As developed formally by Krems and Dalgarno [39], the spin-rotation interaction $\gamma_{SR}\mathbf{N}\cdot\mathbf{S}$ is just such a mechanism. It can couple states with the same value of the sum $M_S + M_N$, which are the projections of the molecular spin and rotation on the lab-fixed Z-axis. This can be seen immediately with the use of the following identity:

$$H_{SR} = \gamma_{SR}\mathbf{N}\cdot\mathbf{S} = \gamma_{SR}\left(N_Z S_Z + \frac{1}{2}\left(N_+ S_- + N_- S_+\right)\right). \tag{8}$$

The inner product $\mathbf{N}\cdot\mathbf{S}$ depends on the relative projection of $\mathbf{N}$ and $\mathbf{S}$, so all states with the same value of $M_J \equiv M_S + M_N$ also have the same energy under the $\gamma_{SR}\mathbf{N}\cdot\mathbf{S}$ interaction and can be coupled by it. It can be seen that for the rotational ground state, $N = 0$, $M_N = 0$ and thus the spin-rotation interaction cannot change M_S without changing M_J. Since M_J is a good quantum number, collisions between helium atoms and $^2\Sigma$ molecules in their rotational ground state cannot directly cause spin-depolarization (first-order perturbation theory predicts a Zeeman transition probability of zero).

Despite these considerations, Krems and Dalgarno have pointed out [39] that there is a three-step process by which the electrostatic interaction of the colliding helium atom and the spin-rotation interaction in the molecule can cause spin depolarization. Even though the electrostatic interaction cannot couple to the electron spin, electric fields can mix rotational states. That means that the helium atom can perturb the rotational state distribution from pure $N = 0$ into a mixture of N states during the collision. In the second step, the spin-rotation interaction can mix in different M_S states from the $N > 0$ portion of the rotational eigenstate that is perturbed by the proximity of the helium atom. Finally, the electrostatic

interaction between the helium atom and these mixed states has off-diagonal elements in M_J, which lead to spin-depolarization.

The first cold molecule trapping was performed with a $^2\Sigma$ molecule, CaH [68]. About 10^8 molecules were loaded into a magnetic trap using buffer-gas loading. The ratio γ of the He-CaH elastic collision cross section to the Zeeman relaxation cross section was measured to be $\gamma \geq 10^7$ [68, 66, 70][3]. Thermal isolation of the trapped species by cooling the cell walls to cryopump the buffer gas was unsuccessful due to the long pump out time required (~ 10 s) compared to the evaporation limited lifetime, which illustrates the importance of a fast traversal of the "Valley of Death" in Fig. 5. Species with a magnetic moment much higher than one Bohr magneton (the case of CaH), such as Cr and Eu, were thermally isolated by cooling the trap walls to lower the vapor pressure of helium. This worked because they experienced a deeper trap during the pump-out and therefore suffered less loss due helium-induced evaporation while traversing the "Valley of Death." Another $^2\Sigma$ molecule, CaF, was also buffer-gas cooled and we measured $\gamma = (1.3 + 1.3/-0.5) \times 10^4$ [41], which was likely dominated by the nonzero thermal population of $N = 1$ rotationally excited molecules.

2.2.2 Inelastic collisions of $^3\Sigma$ molecules with He

The low trap depth that $^2\Sigma$ molecules experience leads to difficulty in the attempt to achieve thermal isolation due to the required speed for buffer-gas removal. Since technological constraints currently limit the maximum magnetic trap depths to around 4 Tesla, it makes sense to pursue molecules with larger magnetic moments to utilize the effectively deeper traps. For this and other reasons, extension of this type of study to $^3\Sigma$ molecules is a natural next step.

The mechanism described above developed by Krems and Dalgarno [39] will still be present for $^3\Sigma$ molecules. As they have pointed out, however, the addition of the spin-spin interaction in $^3\Sigma$ molecules leads to another relaxation channel that tends to dominate the spin depolarization.

The rotational ground state of a $^3\Sigma$ molecule, unlike a $^2\Sigma$, is not a pure $|N = 0\rangle$ state, even in zero field. This is due to the spin-spin interaction, which can be written as

$$H_{\mathrm{SS}} = -\frac{2}{3}\lambda_{\mathrm{SS}}\sqrt{6}\sum_q (-1)^q \sqrt{\frac{4\pi}{5}} \mathrm{Y}_{2,-q}(\theta,\phi)\mathsf{T}^{(2)}_q\left[\mathbf{S},\mathbf{S}\right] \tag{9}$$

where λ_{SS} is the spin-spin coefficient and $\mathsf{T}^{(2)}_q\left[\mathbf{S},\mathbf{S}\right]$ is the spherical tensor product of $\mathbf{S}$ with itself [48]. The $\ell = 2$ spherical harmonics in Eq. 9 connect states with different spin projections and rotational quantum numbers that differ by $\Delta N = 2$. The spin-spin interaction therefore mixes in some $N = 2$ character into the rotational ground state:

$$|\psi, M_J\rangle \propto |N = 0, M_S\rangle + \frac{\lambda_{\mathrm{SS}}}{6B_{\mathrm{e}}}\sum c' \,|N = 2, M'_N, M'_S\rangle \tag{10}$$

where B_{e} is the rotational constant. Here it can be seen mathematically that the spatial orientation of the internuclear axis in the lab frame is coupled to the projection of the electron spin through the spin-spin interaction, even before the helium interacts with the molecule.

[3] A more recent analysis of the data gives this value, which is larger than that quoted in Refs. [68, 66, 70].

The amount of $N = 2$ present depends on the ratio λ_{SS}/B_e. The helium collision induced Zeeman relaxation of $^3\Sigma$ molecules in the zero-field limit is therefore expected to scale as the square of this ratio [39]:

$$\sigma_{ZR} \propto |\langle \psi, M_J | V_{He} | \psi, M_J' \rangle|^2 \propto \frac{\lambda_{SS}^2}{B_e^2}. \tag{11}$$

In light of this scaling law, it is desirable for buffer-gas loading that a $^3\Sigma$ molecule have a large rotational constant and small spin-spin coefficient to minimize the helium interaction anisotropy and therefore the helium-induced Zeeman relaxation. This realization was one of the factors that led our group to the imidogen (NH) radical.

This spin-spin driven helium-induced Zeeman relaxation is likely to be the dominant relaxation mechanism for molecules for which the spin-spin coefficient (λ_{SS}) is larger than the spin-rotation coefficient (γ_{SR}). It is not clear from this qualitative model whether the additional 1 μ_B of magnetic moment gained in moving from $^2\Sigma$ molecules to $^3\Sigma$ states is worth the trouble. If the spin-spin driven Zeeman relaxation of $^3\Sigma$ molecules is too strong, the trap lifetime will be substantially limited by inelastic collisions and not the trap depth. In 2003, a quantitative calculation was performed by Krems *et al.* that predicted a favorable Zeeman relaxation rate coefficient for imidogen (NH) with helium [13, 40]. Furthermore, experiments performed in our group indicate that thermal isolation of $2\mu_B$ species is dramatically easier than $1\mu_B$ [29].

Experimentally, our group demonstrated the first trapping of $^3\Sigma$ polar molecules by buffer-gas loading more than 10^8 imidogen radicals into a magnetic trap directly from a molecular beam [12]. We found that imidogen does have favorable collisional properties for buffer-gas loading. By measuring the trap lifetime for a range of ^{3}He buffer-gas densities, we found a ratio of $\gamma = 7 \times 10^4$, which is sufficiently large to observe trap lifetimes approaching 1 s.

Nonetheless, there is reason to believe that this ratio is lowered by the presence of a shape resonance. Krems and coworkers [13, 40] have predicted an $l = 3$ shape resonance between imidogen and ^{3}He in the collision energy range around 0.5 K. Furthermore, our single-point measurement only partially supports the spin-spin interaction driven relaxation mechanism described below. To investigate these issues further, we first changed the buffer-gas isotope to ^{4}He, for which the $l = 3$ level is a true bound state and therefore no longer corresponds to a shape resonance. We found that the imidogen-^{4}He system has a collision induced Zeeman relaxation cross section about four times smaller than the more standard ^{3}He, supporting the shape resonance prediction. Furthermore, by changing isotopomers of NH (*e.g.* switching from NH to ND) we were able to verify the $1/B^2$ dependence of the Zeeman relaxation cross section for the imidogen-^{4}He system [11].

3 Buffer-gas beam production

Buffer-gas cooling has been used to create cold molecular and atomic beams and demonstrated to produce higher fluxes of cold molecules than any other source. The general approach is to buffer-gas cool the target species in a centimeter-sized cryogenic cell that has

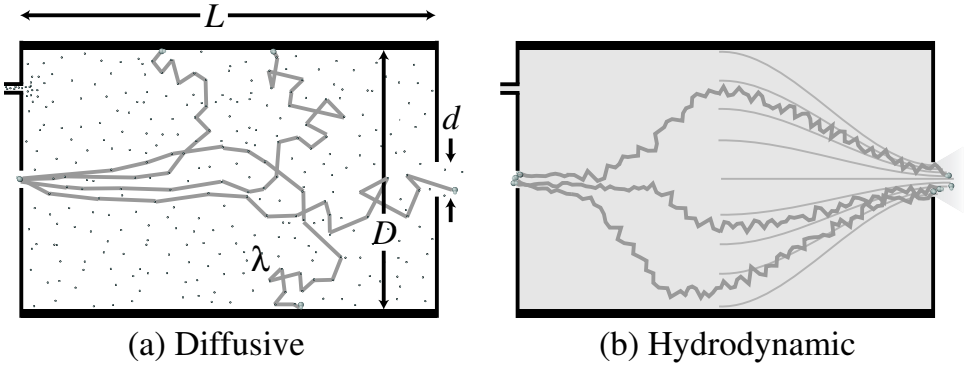

Figure 11: A schematic of a simple buffer gas beam source being operated under (a) diffusive and (b) hydrodynamic cell conditions.

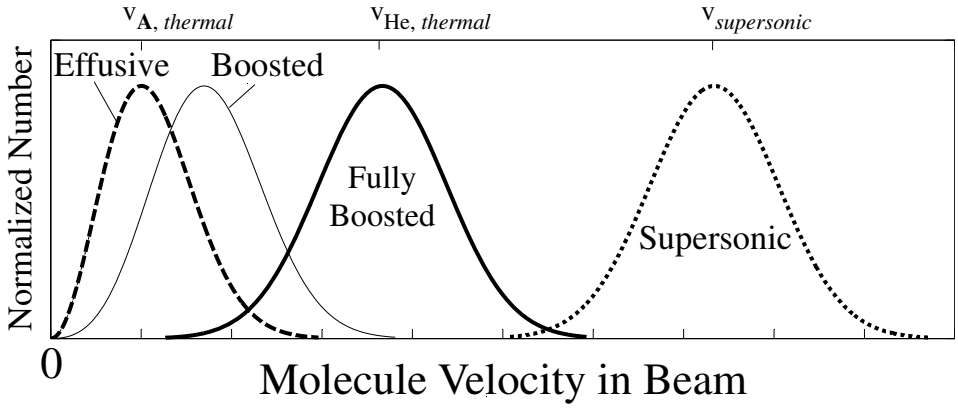

Figure 12: Velocity distributions of a buffer-gas beam operated in four different forward velocity regimes. All four have roughly the same velocity spread, corresponding to $v_{\mathbf{A},thermal}$.

an exit hole with a diameter on the order of mm to cm. Some of the cold target species will exit the hole, either effusively or "boosted", depending on the experiment geometry and density of helium in the cell. Each regime has its peculiar features, as we discuss below.

A simple outline of the operation of a buffer-gas beam source is as follows, and is depicted in Fig. 11. Cold helium gas at temperature T is introduced into a buffer-gas-filled cryogenic cell that is also at temperature T. The cell is a tube with diameter D and length $L \geq D$. At one end (typically opposite the buffer gas entry location) there is an exit hole of diameter d. The helium density $n_{\rm He}$ is held constant by continuously flowing cold helium gas to replenish that lost through the exit hole. Hot particles (atoms or molecules) of target species, **A**, are also introduced into the cell at a location we designate as the target species "entrance point." Generally, the entrance point is at the end of the cell opposite the exit hole (*i.e.* closer to where the buffer gas enters), as shown in Fig. 11.

3.1 Thermalization and extraction conditions

The hot particles of **A** can come arbitrarily close to equilibrium with the buffer gas after a characteristic number of collisions $\mathcal{N}$. Typically, $\mathcal{N} \approx 100$ collisions are sufficient for thermalization to 4 K, as discussed in section 1. The particle's mean free path is given by $\lambda_t = 1/\sqrt{2} n_{\rm He} \sigma_t$ where σ_t is the thermal average of the diffusion cross section. The thermalization time is given by $\tau_{therm} = \mathcal{N}\lambda_t / \bar{\rm v}_{\mathbf{A},cooling}$ where $\bar{\rm v}_{\mathbf{A},cooling}$ is the microscopic velocity of particles of **A** averaged over the temperature range they experience during the thermalization process. The particle's thermalization length can be written as $R_{therm} = \alpha \lambda_t$ where, according to simulations, α varies between $\sqrt{\mathcal{N}}$ and $\mathcal{N}$, depending upon the initial conditions of the particles of **A**. For full thermalization, the cell must be large enough to satisfy $D \geq R_{therm}$. For the purposes of this discussion we will assume that this thermalization condition is always fulfilled.

Fully thermalized particles of **A** can leave the cell volume by two processes: by diffusing to the boundaries of the cell or by being entrained in the helium flow and hydrodynamically pulled out of the exit hole. In order to determine which regime is applicable, the timescales for each process need to be compared.

After thermalization, the particle's macroscopic longitudinal velocity coincides with the flow velocity of helium through the cell, given by $V_{flow} \approx (d/D)^2 {\rm v}_{{\rm He},thermal}$. The time it takes for particles of **A** to traverse the cell at this macroscopic helium flow velocity is given by $\tau_{pumpout} = L/V_{flow}$.

The radial motion of fully-thermalized **A** particles, on the other hand, is diffusive. The diffusion lifetime is given by

$$\tau_{diffusion} = \frac{D^2}{4\lambda_{\rm c} {\rm v}_{\mathbf{A},thermal}} \tag{12}$$

where D is the cell diameter (*not* the diffusion constant), $\lambda_{\rm c}$ is the cold mean free path, given by $\lambda_{\rm c} = 1/n_{\rm He}\sigma_{\rm c}\sqrt{1 + m_{\mathbf{A}}/m_{\rm He}}$ and ${\rm v}_{\mathbf{A},thermal}$ is the cold thermal velocity of the particles of **A**.

The dimensionless parameter

$$\xi \equiv \frac{\tau_{diffusion}}{\tau_{pumpout}} \tag{13}$$

provides a quantitative characterization of which limit the system is in, with $\xi \ll 1$ indicating *diffusive* and $\xi \gg 1$ *hydrodynamic* cell conditions (see Fig. 11). We note that the entrainment being discussed here is *not* the same as that seen in typical supersonic nozzle expansions where it is collisions *within* and just outside the nozzle that play the key role, and flow velocities are comparable to the sonic velocity. The mean flow velocity of helium within the buffer-gas cell is substantially less than the sonic velocity since, in general, $d < D$. For full thermalization of hot particles of **A** to take place, it must be that $\tau_{therm} < \tau_{diffusion}$ for diffusive cell conditions and $\tau_{therm} < \tau_{pumpout}$ for the hydrodynamic regime.

If $\xi \ll 1$, then hydrodynamic effects can be ignored. In this diffusive limit, most of the **A** particles stick to the cell walls. In this case, the fraction of thermalized particles that exit the hole is set by the solid angle coverage fraction of the exit aperture and is generally much less than 1. If $\xi \gg 1$ then a large fraction of **A** particles can be entrained *inside* the cell and be forced by the helium wind to move toward the exit hole and into the beam. Exact analysis depends on the geometrical details, but it can be shown that for $D \approx L$

$$\xi = \frac{\kappa d^2}{4\lambda D} = \frac{\kappa d^2 n_{\mathrm{He}} \sigma_{\mathrm{c}}}{4D} \sqrt{1 + m_{\mathbf{A}}/m_{\mathrm{He}}} \tag{14}$$

with κ a dimensionless constant on the order of unity.

3.2 Boosting condition and slow beam constraints

The forward velocity, $\mathrm{v_F}$, of the beam of **A** particles depends on n_{He} and d, and can be between $\mathrm{v}_{\mathbf{A},thermal}$ and $\mathrm{v}_{supersonic}$. Specifically, $\mathrm{v_F}$ is determined by the Reynolds number (or Knudsen number, $\mathcal{R}_e = 1/\mathrm{Kn}$) for the orifice, $\mathcal{R}_e = d/\lambda$. In the effusive limit, $\lambda \gg d$ and $\mathrm{v_F} \approx \mathrm{v}_{\mathbf{A},thermal}$, as shown in Fig. 12. The **A** particles' trajectories outside the exit hole experience no further collisions.

By contrast, when $\lambda \ll d$, the **A** particles are "boosted" because the outward flow of He outside the exit hole causes collisions with **A** particles, boosting them to higher forward velocities. This causes $\mathrm{v_F}$ to increase from $\mathrm{v}_{\mathbf{A},thermal}$ to $\mathrm{v}_{boosted}$ as $\mathcal{R}_e$ is increased from 1 to >100. Note that the regime of $1 < \mathcal{R}_e < 100$ is often called the intermediate regime in room temperature supersonic nozzle work, whereas $\mathcal{R}_e > 1000$ is called fully supersonic. A fully supersonic expansion is *not* necessary to produce high boosts.

It turns out that the conditions are such that a buffer-gas beam extracted in the hydrodynamic regime will be boosted, meaning that the forward velocity of the molecules will be higher than their mean thermal velocity. This can be seen by noting that for $\xi > 1$, Eq. 14 can be expressed

$$\mathcal{R}_e > D/d \tag{15}$$

where we note that D/d is always greater than 1. Nonetheless, the huge flux enhancement attained by running hydrodynamically (as opposed to diffusively) makes this alternative attractive for certain experiments. The choice between running a cold beam source with diffusive vs. hydrodynamic cell conditions depends on the specific experimental goals. A hydrodynamically-extracted beam yields about a factor of 1000 higher flux than a beam made from a diffusive-mode cell, but the forward velocity is higher, around 100 m s^{-1} for a 4 K cell. On the other hand, an effusive cold beam (which must be extracted under diffusive

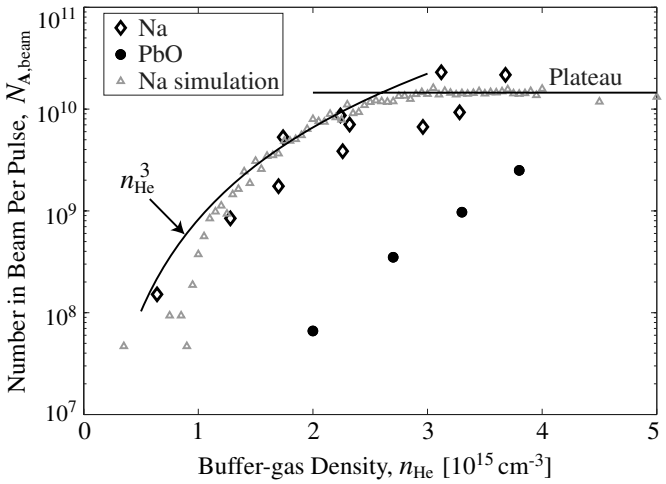

Figure 13: The number of cold **A** particles, $N_{\mathbf{A},\mathrm{beam}}$, that emerge in the beam as a function of the buffer-gas density (n_{He}) in the diffusive cell regime. Curves with specific functional forms have been inserted to show the different scaling regimes. Figure reprinted with permission from [42]. Copyright 2005 by the American Physical Society.

cell conditions) can have forward velocities as low as around 10 m s^{-1}, corresponding to forward kinetic energies 100 times lower than a hydrodynamically-extracted beam.

3.3 Studies with diffusively-extracted beams

The diffusive regime was studied in detail using PbO molecules and Na atoms. A full description is given in reference [42]. The basic layout of the beam apparatus is shown in Fig. 11(a). The buffer-gas cell is a brass box ∼10 cm on edge. The exit hole has $d = 3$ mm and is centered on one side face. Several ablation targets are mounted on the inside top face of the cell about 6 cm from the exit aperture. Na atoms are ablated from sodium metal or NaCl targets, and PbO molecules are ablated from a vacuum hot-pressed PbO target. Buffer gas continuously flows into the cell. Good vacuum is maintained in the beam region by means of a charcoal sorption pump with a pumping speed for helium of ∼1000 l s^{-1}.

For this particular cell, using an assumed cold diffusion cross section $\sigma_{\mathrm{c}} \approx 3 \times 10^{15}$ cm^{-3}, the crossover between effusive and boosted flow (the condition $d = \lambda$) occurs for $n_{\mathrm{He}} \approx 10^{15}$ cm^{-3}. We characterize the beam source for both species within a range of densities around the anticipated optimal condition for Na, namely $n_{\mathrm{He}} \approx 0.2 - 5 \times 10^{15}$ cm^{-3}.

For Na, in-cell laser absorption spectroscopy is used to determine the number of thermalized Na atoms, N_{Na}, and the cold collision diffusion cross section, $\sigma_{\mathrm{c,Na}}$. We find $N_{\mathrm{Na}} \approx 10^{14}$/pulse for both the metallic sodium and NaCl ablation targets. We measure diffusion lifetimes of $\tau\,[\mathrm{ms}] \approx 4 \times 10^{-15} \times n_{\mathrm{He}}\,[\mathrm{cm}^{-3}]$. From this we infer $\sigma_{\mathrm{c,Na}} \approx 3 \times 10^{-15}$ cm^2. Previous work with PbO has measured an ablation yield of $\approx 10^{12}$/pulse [20], and our in-cell LIF measurements indicate a comparable yield.

In Fig. 13 we plot the number, $N_{\mathbf{A},\mathrm{beam}}$, of thermalized particles of species **A** exiting the hole as a function of n_{He}. The ablation plume is not directed at the aperture in order to

ensure that particles only exit the cell and form a beam by first colliding with the cold buffer gas. We can therefore monitor the thermalization of the ablated particles by looking for their appearance in the beam. In the Na data and simulations, we find that $N_{\mathbf{A},\mathrm{beam}}$ increases rapidly (approximately $\propto n_{\mathrm{He}}^3$) up to a critical value of n_{He}, above which $N_{\mathbf{A},\mathrm{beam}}$ is roughly constant at its maximum value. The low-density n_{He}^3 scaling is consistent with a simple picture in which $\mathbf{A}$ particles are uniformly distributed over a volume of $R_{therm}^3 \approx (\mathcal{N}\lambda)^3$ after a near thermalization to T. The intersection of the solid curves corresponds to the condition where the thermalization length matches the distance between the ablation target and the aperture. This saturation corresponds to a maximum fraction in the beam (f_{max}) given by the fractional solid angle of the aperture compared to the rest of the cell, indicating that the motion of particles of $\mathbf{A}$ in the cell is fully diffusive and randomized. For this cell geometry we have $f_{max} \approx 3 \times 10^{-4}$.

The condition for full thermalization (i.e. all of the hot Na produced is thermalized to a temperature close to T) is apparent in both the experimental and simulated data for Na. We find that the highest effusive-regime helium density is almost exactly equal to the density necessary for thermalization of an ablated sample of Na. Thus it should be anticipated that this cell is near the optimal geometry for producing a maximal flux of slow (effusive), cold Na. By contrast, the different initial conditions produced by the ablation of PbO makes the helium density necessary for thermalization larger than for Na, implying that our cell geometry is not optimal for PbO. Nonetheless, we find the translational and rotational temperature of the PbO in the beam is close to T since beam particles are produced only through collisions with buffer-gas atoms.

In order to verify that the cell is being operated in the diffusive regime, we can calculate ξ. The emptying time of the cell can be calculated using the known cell and exit hole sizes. For this cell, this results in a pumpout time of $\tau_{pumpout} = 100$ ms, which is longer than the 1-10 ms diffusion times for the buffer gas densities accessed in these experiments. This verifies that this work is strongly in the diffusive cell regime, i.e. $\xi \ll 1$.

Fig. 14 shows the average forward velocity, $\mathrm{v_F}$, of the beams of $\mathbf{A}$ particles as the buffer-gas density n_{He} is varied. For both Na and PbO, the data show a linear increase of $\mathrm{v_F}$ with n_{He}. Here we can see that for this diffusive regime source, the output beam can be tuned all the way from effusive to strongly boosted (see Fig. 12). The linear increase of $\mathrm{v_F}$ with buffer-gas density is consistent with the following simple picture: a slowly-moving particle of $\mathbf{A}$ takes a time t_{e} to exit the hole, where $t_{\mathrm{e}} \sim d/\mathrm{v}_{\mathbf{A}}$; during this time, it undergoes N_{e} collisions with fast, primarily forward-moving He atoms, where $N_{\mathrm{e}} \sim n_{\mathrm{He}}\sigma_{\mathrm{c}}\mathrm{v}_{\mathrm{He}}t_{\mathrm{e}}$, resulting in a net velocity boost given by $\Delta\mathrm{v}_{\mathbf{A}} \sim \mathrm{v}_{\mathbf{A}}d/\lambda \propto n_{\mathrm{He}}$. This picture should be roughly valid for densities below the fully supersonic regime. The velocities we measure for Na are approximately reproduced by modeling the beam formation process with our measured value of σ_{c}.

3.4 Studies with hydrodynamically-extracted beams

The cell used for our studies of hydrodynamically-extracted beams is smaller than that used in the diffusive regime beam studies, making it possible to achieve $\xi = 1$ while still operating in the convenient $n_{\mathrm{He}} \approx 10^{15}$ cm^{-3} region. The heart of the experimental apparatus is a $\approx$

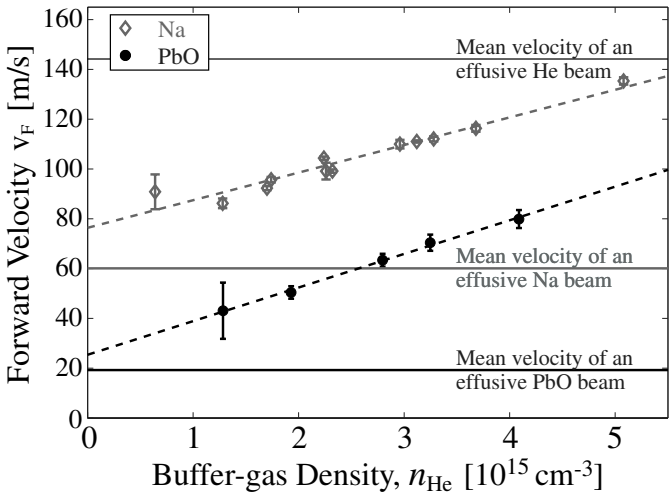

Figure 14: PbO and Na beam mean forward velocities, v_F, as a function of buffer-gas density n_{He}. Extrapolation of the data to zero buffer-gas density is illustrated by best-fit lines (dashed). Figure reprinted with permission from [42]. Copyright 2005 by the American Physical Society.

2.5 cm size cell anchored to the cold plate of a cryostat. This cell is a copper box with two fill lines (one for helium and one for molecular oxygen) on one side, the exit aperture on the opposite side, a Yb ablation target inside, and windows for laser access. With this cell, we make beams of either atomic Yb or O_2. In order to produce beams of O_2, we flow He and O_2 continuously into the cell where they mix and thermalize to the temperature of the cell. To produce beams of Yb, we flow He continuously into the cell and ablate the Yb target with a pulsed YAG laser. Helium typically flows into the cell at 1×10^{17}- 8×10^{18} atom s^{-1}. Despite the large He gas flow, the vacuum in the beam region is maintained at a low 3×10^{-8} torr by two stages of differential pumping with high speed cryopumps made of activated charcoal.

We run two different types of experiments with this cell, either magnetically guided (with O_2) or unguided (with Yb). In the guided work, we couple O_2 into a magnetic guide and measure the flux of O_2 exiting the guide with a residual gas analyzer (RGA). This work is described in detail in Ref. [56] and we direct the reader there. In the unguided work, we use Yb to characterize the beam source. The flux and velocity profile of the Yb beam and the density and temperature of the Yb gas in the cell are all measured using laser absorption spectroscopy.

Two exit hole configurations were demonstrated to produce Yb beams. Fig. 15 shows the output efficiency of a simple slit aperture (1 mm x 4 mm), where this efficiency is defined as the ratio of the number of Yb in the beam to the number of cold Yb produced by ablation in the cell. At high buffer-gas flows, $\xi > 1$ (the hydrodynamic cell regime) and up to 40% of the cold Yb atoms in the cell are detected in the resultant beam. The divergence of the beam is measured by comparing the Doppler shifts in the absorption spectra parallel and transverse to the atomic beam. The beam is more collimated than a pure effusive source, with a divergence of ≈ 0.1 steradian. This observed effect of angular peaking of the beam has been seen in room temperature beam experiments using two species of different mass and is

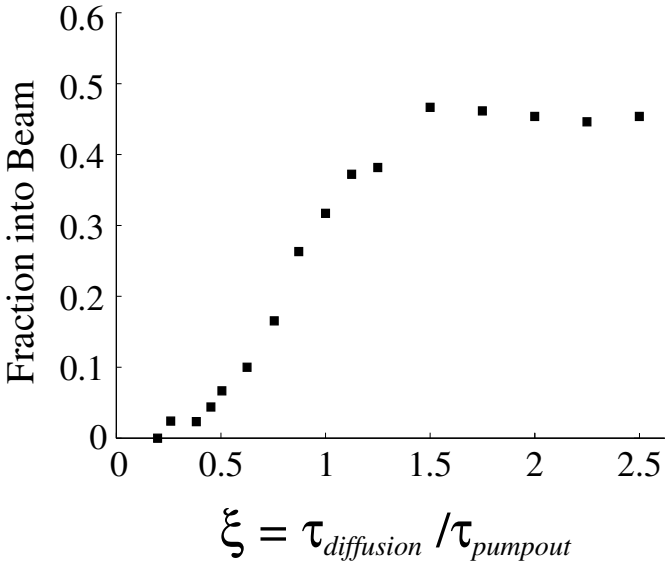

Figure 15: Plotted is the ratio of the number of ablated and cooled ytterbium atoms to the number emitted into the beam for a simple slit aperture (no suppressor nozzle). At high buffer-gas densities, which correspond to long diffusion times and therefore high ξ (see main text), up to 40% of the cold ablated atoms are detected in the peak instantaneous flux represented here of 5×10^{15} atom s^{-1} sr^{-1}. Reprinted with permission from [56].

often called "Mach-number focusing" [1, 65]. The higher mass species has its angular beam distribution narrowed due to the same boosting effect described earlier – the light species knocks the heavy species from behind, randomizing its transverse motion while always kicking it forward. This effect peaks in the middle of the intermediate regime, $\mathcal{R}_e \approx 30$, becoming much less pronounced as one approaches either the effusive or fully supersonic regime. A peak on-axis flux per unit solid angle of 6×10^{15} atom s^{-1} sr^{-1} (5×10^{12} atoms/pulse) has been measured.

For trapping, where total kinetic energy of the trappable species must be less than the trap depth (typically a few Kelvin) the high forward velocity of a boosted beam ($v_F = 130$ m s^{-1} $>$ 100 K effective temperature for Yb) makes it unsuitable. Trapping work would ideally use a beam with both high flux (available for $\xi > 1$, implying $\mathcal{R}_e > 1$) and v_F as close as possible to $v_{\mathbf{A},thermal}$. In an attempt to achieve the best of the two worlds, we developed a two-stage aperture called the *suppressor nozzle* (by analogy to a suppressor or silencer for a gun, which works much the same way) [56]. With this two stage aperture, the He-Yb mixture still passes through the 1 mm x 4 mm slit out of the buffer-gas cell, resulting in a large hydrodynamic flux enhancement but correspondingly boosted forward velocity ($v_F > v_{\mathbf{A},thermal}$). To suppress this boost of the forward beam velocity while maintaining the high brightness provided by the hydrodynamic regime, the cell is fitted with the suppressor nozzle just outside the slit aperture. The suppressor nozzle consists of a small chamber with a large exit hole opposite the cell slit. This second, larger exit hole is covered by a stainless steel mesh with pore size 140 microns (28 percent transparency) and creates a near-effusive beam (actually a large number of near-effusive beams in parallel) in the vacuum region,

where there are no more collisions. The He density in the suppressor nozzle volume would be far too low to thermalize hot atoms entering the cell. However, this density is high enough to collisionally slow the internally-cold (but forward boosted) Yb that comes through the first orifice and low enough so that $\xi \ll 1$, *i.e.* diffusion dominates the dynamics. In this sense, the suppressor nozzle itself is a small buffer-gas cooling cell operated in the diffusive cell regime.

The Yb beam from the suppressor nozzle has a mean velocity of 35 m s^{-1}, with a spread of 20 m s^{-1}. The measured peak on-axis beam flux of 5×10^{12} atom s^{-1} sr^{-1} represents about 1% of the cold atomic Yb produced in the ablation, or about 3% of the output of the one-stage aperture (compare to 0.03% for the diffusive cell regime).

One of the future directions for producing cold beams is to inject hot molecules along the same direction and into the stream of cold helium gas flowing inside a long tube $L > D$. The tube length would be set so that particles of **A** would diffuse a distance $D/2$ in a time L/V_{flow} for a helium density set so that $n_{\mathrm{He}} = \Upsilon n_{\mathbf{A}}$, where $n_{\mathbf{A}}$ is the density of particles of **A** and Υ is defined in section 1. The cooling of particles of **A** in such a system could be enhanced with suppressed loss of **A** particles in a case where $\sigma_{\mathrm{He-He}} < \sigma_{\mathrm{He-A}}$.

4 Summary

Buffer-gas cooling of molecules promises to continue to provide researchers with a general method for obtaining gas-phase samples of cold molecules. The applicability of the technique to a wide variety of atoms and molecules has already led to extensions of the fields of magnetic trapping, quantitative spectroscopy, and slow beam creation. Furthermore, due to the fact that buffer-gas cooling accepts the full Boltzmann distribution of the initial molecular sample, the high numbers of molecules that can be cooled with this method (often also translating to high densities or high beam fluxes) exceed other methods, often by orders of magnitude. Since diatomic molecules have rotational splittings that are often of order of 1 K, the use of cryogenic helium buffer gas for collisional cooling is a conceptually straightforward process that seems to fit naturally into the world of diatomic molecules. For many types of experiments, the rotational state population enhancement alone is sufficient to make buffer-gas cooling an attractive option.

Buffer-gas cooling is also useful for experiments requiring certain degrees of freedom to remain out of equilibrium with the buffer-gas temperature, such as magnetostatic trapping and metastable lifetime measurements. It is important to continue to study the collisional thermalization processes in detail to gain a thorough understanding of the relevant mechanisms. We expect the knowledge base that will be developed for cold collisional processes can be applied in the future to sympathetically or evaporatively cool trapped molecules down to the ultracold regime.

Acknowledgments

We would like to acknowledge the many members of the experimental and theoretical groups at Harvard who contributed to the development of buffer-gas cooling. Others who are de-

serving of acknowledgment for advancing the field include F. DeLucia for his pioneering work on collisional cooling, D. DeMille, G. Meijer, A. Peters, M. Stoll, D. Kleppner, T. Greytak, and W. Ketterle. This work was supported by the U.S. NSF, DOE, and ARO.

A Tables of buffer-gas cooled species

Key to the notes in Tables 1 and 2:

(b) Simultaneous metastable and ground state production and observation

(f) ^{15}NH and ^{15}ND also trapped

(g) surface evap down to 2 mK; RF evap to < 100 μK

(h) evap from 160 mK

(i) optical density OD = 1.2

(j) OD = 75

(n) OD = 6

(q) OD > 10

(s) flux in a 100 ms pulse

(t) $\gamma = 7 \times 10^4$ for ^{3}He

(u) data from [68, 70] were reanalyzed for γ

(v) lifetime limited by spontaneous emission

(w) instantaneous flux over a 3 ms wide pulse

(z) steady state flow of molecules into the cell, we estimate helium densities used equivalent to about 100 ms diffusion life time

References

[1] James B. Anderson. Separation of gas mixtures in free jets. *AIChE Journal*, 13(6):1188–1192, 1967.

[2] Joost M. Bakker, Michael Stoll, Dennis R. Weise, Oliver Vogelsang, Gerard Meijer, and Achim Peters. Magnetic trapping of buffer-gas-cooled chromium atoms and prospects for the extension to paramagnetic molecules. *J. Phys. B*, 39:S1111, 2006.

[3] C. D. Ball and F. C. De Lucia. Direct observation of Λ-doublet and hyperfine branching ratios for rotationally inelastic collisions of NO - He at 4.2 K. *Chem. Phys. Lett.*, 300:227, 1999.

Species	$N/n/F$	T [K]	Result	τ [s]	$\gamma[\times 10^4]$	Loading	Notes	Ref.
CaF	5E13	2	cold	0.08	1.3	ablation	-	[41, 21]
CaH	1E8; n = 8E7	0.40	trap	0.50	10^3	ablation	u	[68, 70]
CH_3F	$n \leq$ 2E13	1.2	cold	-	-	capillary	z	[19, 7]
CrH	1E5; n = 1E6	0.65	trap	0.12	0.9	ablation	-	[62]
CO	$n \leq$ 5E12	1.3	cold	-	-	capillary	-	[74, 6]
DCl	$n \leq$ 5E12	1.85	cold	-	-	capillary	z	[73]
H_2S	$n \leq$ 5E12	1	cold	-	-	capillary	z	[72, 4]
H_2CO	$n \leq$ 1E13	1.7	cold	-	-	capillary	z	[44]
HCN	$n \leq$ 7E13	1.3	cold	-	-	capillary	z	[60]
MnH	1E5; n = 1E6	0.65	trap	0.18	0.05	ablation	-	[62]
ND	1E8	0.55	trap	0.50	7	from beam	f	[11, 9]
NH	5E11	4	cold	-	-	from beam	-	[12]
	2E8	0.55	trap	0.95	20	from beam	f, t	[17]
($v = 1$)	2E7	0.615	trap	0.033	> 5	from beam	v	[10, 9]
ND_3	F = 1E15	7	beam	-	-	capillary	-	[58]
	F = 1E12	7	guide	-	-	capillary	-	[58]
NO	$n \leq$ 2E12	1.8	cold	-	-	capillary	z	[71, 3]
O_2	F = 3E12	1.6-25	guide	-	-	capillary	-	[56]
PbO	1E12	4	cold	0.020	-	ablation	-	[21]
PbO	F = 1E9	4	cold	-	-	ablation	-	[42]
SrO	2E12	4	cold	>0.02	-	ablation	-	[15]
	F = 1E13		beam	-	-	ablation	-	[15]
	F = 5E10		guide	-	-	ablation	-	[15]
ThO	1E13	4	cold	0.03	-	ablation	b	[63]
	F = 1E15		beam	-	-	ablation	w	[63]
VO	1E12	1.5	cold	0.06	-	ablation	-	[70]

Table 1: This table contains a list of molecules that have been helium buffer-gas cooled to less than 10 K. $N/n/F$-The number(s) in this column are maximum number, density or flux, in units of N[none], n[cm^{-3}], and F[s^{-1}]. T- lowest temperature reached with this species in a helium buffer-gas based experiment. This temperature does not necessarily correspond to the maximum number or density given in the $N/n/F$ column. In the case of trapping this temperature indicates the lowest trapped temperature achieved. In the case of a beam, it generally indicates the transverse temperature of the beam. Result indicates whether the molecules were just cooled or cooled and trapped, made into a beam, or made into a guided beam. τ is the maximum lifetime observed. In the case of trapping, this is the approximate maximum lifetime observed in the trap. γ is the ratio of diffusion to spin relaxation cross section. $\gg$ indicates that γ was very high and no spin relaxation was observed, and "nm" indicates that γ was observed to be low but was not measured. Loading refers to the method used to introduce species into the buffer gas—either laser ablation, capillary injection, LIAD, or loading from a beam. The key to the Notes column is given in the text.

Species	$N/n/F$	T [K]	Result	τ [s]	$\gamma[\times 10^4]$	Loading	Notes	Ref.
Ag	4E13	0.42	trap	2.3	300	ablation	-	[8]
Au	1E13	0.40	cold	0.12	>10	ablation	-	[8]
Bi	5E11	0.50	cold	0.09	<4	ablation	-	[43]
Ce	1E12	0.60	cold	0.08	4	ablation	q	[49]
Cr	1E12; n = 1E13	<0.01	trap	>100	$\gg$	ablation	-	[69, 46]
Cr	1E11; n = 1E12	0.35	trap	60	$\gg$	ablation	-	[2]
Cs	2E9	4	cold	0.002	-	ablation	-	[55]
Cu	3E12	0.32	trap	8	800	ablation	-	[8]
Dy	2E12	0.60	trap	> 20	50	ablation	-	[27]
Er	2E11	0.80	trap	0.05	4	ablation	-	[27]
Eu	1E12; n = 5E12	0.25	trap	>100	$\gg$	ablation	-	[36]
Fe	5E11	0.60	cold	<0.01	<0.5	ablation	-	[35]
Gd	1E10	0.80	cold	0.07	nm	ablation	-	[28]
He*	5E11; n = 5E11	<0.001	trap	$\gg$100	$\gg$	discharge	g	[50, 16]
Hf	1E12	0.35	cold	0.00?	<0.3	ablation	-	[51]
Ho	1E10	0.60	trap	4	nm	ablation	-	[49]
Ho	9E11	0.80	trap	> 20	30	ablation	-	[27]
K	4E9	4	cold	0.008	-	ablation	-	[55]
Li	2E13; n = 2E12	0.09	cold	100	$\gg$	ablation	h	[14]
Mn	2E12	0.85	trap	>100	$\gg$	ablation	-	[52, 54]
Mo	2E10	0.20	trap	>100	$\gg$	ablation	-	[24]
N	1E11; n = 5E12	0.55	trap	12	$\gg$	from beam	-	[34]
Na	F = 1E15	4	cold	-	-	ablation	s	[42]
	5E12	0.48	trap	0.3	$\gg$	ablation	-	[53]
Nd	1E12	0.80	trap	1	9	ablation	-	[27]
Ni	1E13	0.60	cold	0.02	1	ablation	n	[35]
Pr	3E11	0.80	trap	0.12	10	ablation	-	[27]
Rb	n = 1.5E11	4.5	cold	0.018	-	ablation	j	[32]
Rb	1.2E12; n = 8E9	4	cold	-	-	from beam	i	[21]
Rb	n = 1E9	1.85	cold	10	-	LIAD	-	[31]
Re	1E12	0.50	cold	0.45	<30	ablation	-	[43]
Sc	1E11	0.80	cold	0.14	<1.6	ablation	-	[26]
Tb	2E11	0.80	trap	0.12	10	ablation	-	[27]
Ti	4E10	0.80	cold	0.15	~ 4	ablation	-	[26]
Tm	2E11	0.80	trap	0.03	3	ablation	-	[27]
Y	1E11	0.80	cold	0.18	<3	ablation	-	[25]
Yb	2E13	4	cold	0.10	-	ablation	-	[56, 57]
	F = 5E14		beam	-	-	ablation	-	[56]
Zr	1E10	0.80	cold	0.10	nm	ablation	-	[25]

Table 2: Atoms that have been helium buffer-gas cooled. See caption of Table 1.

[4] Christopher D. Ball and Frank C. De Lucia. Direct measurement of rotationally inelastic cross sections at astrophysical and quantum collisional temperatures. *Phys. Rev. Lett.*, 81(2):305–308, 1998.

[5] Christopher D. Ball and Frank C. De Lucia. Direct observation of Λ-doublet and hyperfine branching ratios for rotationally inelastic collisions of NO-He at 4.2 K. *Chem. Phys. Lett.*, 300:227–235, 1999.

[6] M. M. Beaky, T. M. Goyette, and F. C. De Lucia. Pressure broadening and line shift measurement of carbon monoxide in collision with helium from 1 to 600 K. *J. Chem. Phys.*, 105:3994, 1996.

[7] M.M. Beaky, D. C. Flatin, J. J. Holton, T. M. Goyette, and F. C. De Lucia. Hydrogen and helium pressure broadening of CH_3F between 1 K and 600 K. *J. Mol. Structure*, 352/353:245, 1995.

[8] N. Brahms, B. Newman, C. Johnson, D. Kleppner, T. Greytak, and J.M. Doyle. Magnetic trapping of silver and copper, and anomolous spin-relaxation in the Ag-He system. submitted to PRL.

[9] Wesley C. Campbell. *Magnetic Trapping of Imidogen Molecules*. PhD thesis, Harvard University, 2008.

[10] Wesley C. Campbell, Gerrit C. Groenenboom, Hsin-I Lu, Edem Tsikata, and John M. Doyle. Time-domain measurement of spontaneous vibrational decay of magnetically trapped NH. *Phys. Rev. Lett.*, 100:083003, 2008.

[11] Wesley C. Campbell, Timur V. Tscherbul, Hsin-I Lu, Edem Tsikata, Roman V. Krems, and John M. Doyle. Collision-induced spin depolarization of $^3\Sigma$ molecules. submitted to PRL.

[12] Wesley C. Campbell, Edem Tsikata, Hsin-I Lu, Laurens D. van Buuren, and John M. Doyle. Magnetic trapping and Zeeman relaxation of NH ($X^3\Sigma^-$). *Phys. Rev. Lett.*, 98:213001, 2007.

[13] H. Cybulski, R. V. Krems, H. R. Sadeghpour, A. Dalgarno, J. Kłos, G. C. Groenenboom, A. van der Avoird, D. Zgid, and G. Chałasiński. Interaction of NH($X^3\Sigma^-$) with He: Potential energy surface, bound states, and collisional relaxation. *J. Chem. Phys.*, 122:094307, 2005.

[14] R. deCarvalho, N. Brahms, B. Newman, J. M. Doyle, D. Kleppner, and T. Greytak. A new path to ultracold hydrogen. *Can. J. Phys.*, 83:293–300, 2005.

[15] D. DeMille et al. Cold beam of SrO for trapping studies. unpublished.

[16] S. Doret, C. Connolly, and J.M. Doyle. Ultracold metastable helium, 2008. unpublished.

[17] 2004. See, for example, Euro. Phys. J. D special issue on cold molecules.

[18] John M. Doyle, Bretislav Friedrich, Jinha Kim, and David Patterson. Buffer-gas loading of atoms and molecules into a magnetic trap. *Phys. Rev. A*, 52(4):R2515–R2518, 1995.

[19] R.L. Crownover D.R. Willey, D.N. Bittner, and F. C. De Lucia. Very low temperature spectroscopy: The pressure broadening coefficients for CH_3F between 4.2 and 1.9 K. *J. Chem. Phys.*, 89:6147–6156, 1988.

[20] Dima Egorov, Jonathan D. Weinstein, David Patterson, Bretislav Friedrich, and John M. Doyle. Spectroscopy of laser-ablated buffer-gas-cooled PbO at 4 K and the prospects for measuring the electric dipole moment of the electron. *Phys. Rev. A*, 63:030501(R), 2001.

[21] Dimitri Michael Egorov. *Buffer-Gas Cooling of Diatomic Molecules*. PhD thesis, Harvard University, 2004.

[22] R. C. Forrey, V. Kharchenko, N. Balakrishnan, and A. Dalgarno. Vibrational relaxation of trapped molecules. *Phys. Rev. A*, 59(3):2146–2152, 1999.

[23] M. Goeppert Mayer. Rare-earth and transuarnic elements. *Phys. Rev.*, 60:184–187, 1941.

[24] C.I. Hancox, M.T. Hummon, S.V. Nguyen, and J.M. Doyle. Magnetic trapping of atomic molybdenum. *Phys. Rev. A*, 71:031402, 2004.

[25] Cindy I. Hancox. *Magnetic trapping of transition-metal and rare-earth atoms using buffer gas loading*. PhD thesis, Harvard University, 2005.

[26] Cindy I. Hancox, S. Charles Doret, Matthew T. Hummon, Roman V. Krems, and John M. Doyle. Suppression of angular momentum transfer in cold collisions of transition metal atoms in ground states with nonzero orbital angular momentum. *Phys. Rev. Lett.*, 94:013201, 2005.

[27] Cindy I. Hancox, S. Charles Doret, Matthew T. Hummon, Linjao Luo, and John M. Doyle. Magnetic trapping of rare-earth atoms at millikelvin temperatures. *Nature*, 431:281–284, 2004.

[28] Cindy I. Hancox, S. Charles Doret, Matthew T. Hummon, Linjiao Luo, and John M. Doyle. Buffer-gas cooling of gadolinium. unpublished.

[29] J. G. E. Harris, R. A. Michniak, S. V. Nguyen, N. Brahms, W. Ketterle, and J. M. Doyle. Buffer gas cooling and trapping of atoms with small effective magnetic moments. *Europhys. Lett.*, 67(2):198–204, 2004.

[30] J. B. Hasted. *Physics of Atomic Collisions*, chapter 1.6. American Elsevier Publishing Company, Inc., 2 edition, 1972.

[31] A. Hatakeyama, K. Enomoto, N. Sugimoto, and T. Yabuzaki. Atomic alkali-metal gas cells at liquid-helium temperatures: Loading by light-induced atom desorption. *Phys. Rev. A*, 65:022904, 2002.

[32] T. Hong, J.M. Doyle, M. Lukin, D. Patterson, A. Zibrov, and M. Prentiss. Electromagnetically induced transparency in buffer-gas cooled Rb at 4 K. manuscript in preparation.

[33] Y. H. Huang and G. B. Chen. A practical vapor pressure equation for helium-3 from 0.01 K to the critical point. *Cryogenics*, 46(12):833–839, 2006.

[34] Matthew T. Hummon, Wesley C. Campbell, Edem Tsikata, Hsin-I Lu, Yihua Wang, and John M. Doyle. Magnetic trapping of atomic nitrogen and co-trapping of NH. submitted to PRL, 2008.

[35] C. Johnson, N. Brahms, B. Newman, J. Doyle, D. Kleppner, and T. Greytak. Zeeman relaxation of cold atomic Fe and Ni in collisions with ^{3}He. manuscript in preparation, 2008.

[36] J. Kim, B. Friedrich, D.P. Katz, D. Patterson, J.D. Weinstein, R. deCarvalho, and J.M. Doyle. Buffer-gas loading and magnetic trapping of atomic europium. *Phys. Rev. Lett.*, 78:3665, 1997.

[37] Viatcheslav Kokoouline, Robin Santra, and Chris H. Greene. Multichannel cold collisions between metastable Sr atoms. *Phys. Rev. Lett.*, 90(25):253201, 2003.

[38] R. V. Krems and A. Dalgarno. Disalignment transitions in cold collisions of ^3P atoms with structureless targets in a magnetic field. *Phys. Rev. A*, 68:013406, 2003.

[39] R. V. Krems and A. Dalgarno. Quantum-mechanical theory of atom-molecule and molecular collisions in a magnetic field: spin depolarization. *J. Chem. Phys.*, 120(5):2296–2307, 2004.

[40] R. V. Krems, H. R. Sadeghpour, A. Dalgarno, D. Zgid, J. Kłos, and G. Chałasiński. Low-temperature collisions of NH($X^3\Sigma^-$) molecules with He atoms in a magnetic field: An *ab initio* study. *Phys. Rev. A*, 68:051401(R), 2003.

[41] Kenneth Maussang, Dima Egorov, Joel S. Helton, Scott V. Nguyen, and John M. Doyle. Zeeman relaxation of CaF in low-temperature collisions with helium. *Phys. Rev. Lett.*, 94:123002, 2005.

[42] S. E. Maxwell, N. Brahms, R. deCarvalho, D. R. Glenn, J. S. Helton, S. V. Nguyen, D. Patterson, J. Petricka, D. DeMille, and J. M. Doyle. High-flux beam source for cold, slow atoms or molecules. *Phys. Rev. Lett.*, 95(17):173201, 2005.

[43] S.E. Maxwell, M.T. Hummon, Y. Wang, A.A. Buchachenko, R.V. Krems, and J.M. Doyle. Spin-orbit interaction and collision dynamics of atomic bismuth. manuscript in preparation.

[44] Markus Mengel and Frank C. De Lucia. Helium and hydrogen induced rotational relaxation of H_2CO observed at temperatures of the interstellar medium. *Astrophys. J.*, 543:271–274, 2000.

[45] J. K. Messer and Frank C. De Lucia. Measurement of pressure-broadening parameters for the CO-He system at 4 K. *Phys. Rev. Lett.*, 53(27):2555–2558, 1984.

[46] Robert Michniak. *Enhanced Buffer Gas Loading: Cooling and Trapping of Atoms with Low Effective Magnetic Moments*. PhD thesis, Harvard University, 2004.

[47] Alan L. Migdall, John V. Prodan, William D. Phillips, Thomas H. Bergeman, and Harold J. Metcalf. First observation of magnetically trapped neutral atoms. *Phys. Rev. Lett.*, 54:2596–2599, 1985.

[48] M. Mizushima. *The Theory of Rotating Diatomic Molecules*. Wiley, New York, 1975.

[49] B. Newman, N. Brahms, C. Johnson, D. Kleppner, T. Greytak, and J. Doyle. Buffer-gas cooled cerium. unpublished, 2008.

[50] S. Nguyen, S. Charles Doret, C. Connolly, R. Michniak, W. Ketterle, and J.M. Doyle. Evaporation of metastable helium in the multi-partial-wave regime. *Phys. Rev. A*, 92:060703(R), 2005.

[51] S. V. Nguyen, S. C. Doret, J. Helton, K. Maussang, and J. M. Doyle. Buffer gas cooled hafnium, 2008. unpublished.

[52] S. V. Nguyen, J. S. Helton, K. Maussang, W. Ketterle, and John M. Doyle. Magnetic trapping of an atomic ^{55}Mn-^{52}Cr mixture. *Phys. Rev. A*, 71:025602, 2005.

[53] S. V. Nguyen, R. Michniak, and J. Doyle. Trapping of Na in the presence of buffer gas. 2004.

[54] S.V. Nguyen, J.G.E. Harris, S.C. Doret, J.Helton, R.A. Michniak, W. Ketterle, and J.M. Doyle. Spin-exchange and dipolar relaxation of magnetically trapped Mn. *Phys. Rev. Lett.*, 99, 2007.

[55] M. Parsons, R. Chakraborty, W. Campbell, and J.M. Doyle. Ablation studies. manuscript in preparation, 2008.

[56] D. Patterson and J.M. Doyle. Bright, guided molecular beam with hydrodynamic enhancement. *J. Chem. Phys.*, 126:154307, 2007.

[57] D. Patterson and John M. Doyle. Buffer gas cooled Yb in cell, 2008. unpublished.

[58] D. Patterson, J. Rasmussen, and J.M. Doyle. Guided, cold ammonia. To be published.

[59] Frank Pobell. *Matter and Methods at Low Temperatures*. Springer, 2 edition, 1996.

[60] T. J. Ronningen and F. C. De Lucia. Helium induced pressure broadening and shifting of HCN hyperfine transitions between 1.3 and 20 K. *J. Chem. Phys.*, 122:184319, 2005.

[61] Robin Santra and Chris H. Greene. Tensorial analysis of the long-range interaction between metastable alkaline-earth-metal atoms. *Phys. Rev. A*, 67:062713, 2003.

[62] M. Stoll et al. Trapping and spin relaxation in MnH and CrH, 2008. unpublished.

[63] Amar C. Vutha, O. Keith Baker, Wesley C. Campbell, David DeMille, John M. Doyle, Gerald Gabrielse, Yulia V. Gurevich, and Maarten A. H. M. Jansen. Cold beam of ThO for EDM studies. unpublished.

[64] Thad G. Walker and William Happer. Spin-exchange optical pumping of noble-gas nuclei. *Rev. Mod. Phys.*, 69(2):629–641, 1997.

[65] P. C. Waterman and S. Alexander Stern. Separation of gas mixtures in a supersonic jet. *J. Chem. Phys.*, 31(2):405–419, 1959.

[66] There is a typo in Ref. [68]; the quoted elastic-to-inelastic collision rato should read $\sigma_e/\sigma_s > 10^4$.

[67] Jonathan D. Weinstein, Robert deCarvalho, Karine Amar, Andrea Boca, Brian C. Odom, Bretislav Friedrich, and John M. Doyle. Spectroscopy of buffer-gas cooled vanadium monoxide in a magnetic trapping field. *J. Chem. Phys.*, 109(7):2656–2661, 1998.

[68] Jonathan D. Weinstein, Robert deCarvalho, Thierry Guillet, Bretislav Friedrich, and John M. Doyle. Magnetic trapping of calcium monohydride molecules at milikelvin temperatures. *Nature*, 395:148, 1998.

[69] Jonathan D. Weinstein, Robert deCarvalho, Cindy I. Hancox, and John M. Doyle. Evaporative cooling of atomic chromium. *Phys. Rev. A*, 65:021604(R), 2002.

[70] Jonathan David Weinstein. *Magnetic Trapping of Atomic Chromium and Molecular Calcium Monohydride*. PhD thesis, Harvard University, 2001.

[71] D. R. Willey, D. N. Bittner, and F. C. De Lucia. Collisional cooling of the NO- He system: The pressure broadening cross sections between 4.3 and 1.8 K. *Mol. Phys.*, 66:1, 1988.

[72] D. R. Willey, D. N. Bittner, and F. C. De Lucia. Pressure broadening cross sections for the H_2S - He system in the temperature region between 4.3 and 1.8 K. *J. Molec. Spec.*, 134:240, 1989.

[73] D. R. Willey, V. E. Choong, and F. C. De Lucia. Very low temperature helium pressure broadening of DCl in a collisionally cooled cell. *J. Chem. Phys.*, 96:898–902, 1992.

[74] D. R. Willey, R.L. Crownover, D.N. Bittner, and F. C. De Lucia. Very low temperature spectroscopy: The pressure broadening coefficients for CO-He between 4.3 and 1.7 k. *J. Chem. Phys.*, 89:1923, 1988.